Performance of Advanced Heavy-Lift, High-Speed Rotorcraft Configurations

Wayne Johnson*, Hyeonsoo Yeo**, and C.W. Acree, Jr.*

*Aeromechanics Branch, NASA
**Aeroflightdynamics Directorate (AMRDEC), U.S. Army Research, Development, and Engineering Command
Ames Research Center, Moffett Field, California

Abstract

The aerodynamic performance of rotorcraft designed for heavy-lift and high-speed cruise is examined. Configurations considered include the tiltrotor, the compound helicopter, and the lift-offset rotor. Design conditions are hover and 250-350 knot cruise, at 5k/ISA+20°C (civil) or 4k/95°F (military); with cruise conditions at 4000 or 30,000 ft. The performance was calculated using the comprehensive analysis CAMRAD II, emphasizing rotor optimization and performance, including wing-rotor interference. Aircraft performance was calculated using estimates of the aircraft drag and auxiliary propulsion efficiency. The performance metric is total power, in terms of equivalent aircraft lift-to-drag ratio $L/D = WV/P$ for cruise, and figure of merit for hover.

Keywords: rotorcraft, tiltrotor, compound helicopter, lift-offset, performance

INTRODUCTION

NASA and the U.S. Army at Ames Research Center have recently conducted a number of investigations of the aerodynamic performance capability of rotorcraft designed for heavy-lift and high-speed cruise (Refs. 1 to 6). The motivations for these investigations include the tremendous potential impact of an efficient, large rotorcraft on civil air transportation, and future military requirements for long-range, efficient heavy-lift VTOL aircraft. This paper summarizes the results of these investigations, with emphasis on the performance of rotorcraft designed for heavy-lift and high-speed cruise.

The NASA Heavy Lift Rotorcraft Systems Investigation (Refs. 1 and 2) examined in depth several rotorcraft configurations for large civil transport designed to meet the technology goals of the NASA aeronautics program. The investigation identified the Large Civil Tiltrotor as the configuration with the best potential to meet these goals. The design was economically competitive, with the potential for substantial impact on the air transportation system.

With the increasing interest in large VTOL aircraft for military transport, including the on-going Joint Heavy Lift (JHL) Concept Design and Analysis (CDA) activities, work has continued to explore the aerodynamic capabilities of compound helicopters, and lift-offset configurations, as well as tiltrotor aircraft.

NASA HEAVY LIFT ROTORCRAFT SYSTEMS INVESTIGATION

The Rotorcraft Sector within the Vehicle Systems Program of the NASA Aeronautics Research Mission Directorate established as its objective the improvement of public mobility and access to air transportation. The technology goals of the Sector originated from industry studies and workshops during 2001–2004 that focused on a new class of vehicles known as Runway Independent Aircraft (RIA). References 7–8 showed that RIA can relieve runway and terminal area congestion by replacing small aircraft and short-haul flights that use primary runways. The primary runways would then be used exclusively for larger aircraft and medium/long-haul flights. RIA would operate from stub runways and/or helicopter landing pads. This operational concept would increase the capacity of the air transportation system. Reference 9 describes three RIA configurations analyzed by the rotorcraft industry (see Figure 1): the quad tiltrotor (Bell Helicopter), the reverse velocity rotor concept (Sikorsky), and the tiltrotor (Boeing). The studies identified the benefits of advanced technology and the resulting effects on

operating cost. In summary, Refs. 7–9 provide justification for the overwhelming positive impact that RIA can have on the national air space.

Using the RIA studies as motivation, work was focused enabling technology for a notional civil VTOL transport capable of carrying 120 passengers at a cruise speed of 350 knots at 30,000 ft altitude (Mach number 0.60) with a range of 1200 nm (without refueling). This heavy-lift transport will be "neighborly" quiet when operating near communities, economically competitive with a Boeing 737 aircraft, and will exploit available airspace and ground space (excluding primary runways). Specific mission and technology goals were established to push the state-of-the-art in rotorcraft technology.

The objective of the investigation was to select a heavy-lift rotorcraft system that has the best chance of meeting the goals while being economically competitive. The goals relating to aerodynamically efficient cruise and hover, structural efficiency, and low community noise were given highest priority. A NASA-led team of rotorcraft technologists analyzed three vehicle configurations suggested by the rotorcraft industry: a tiltrotor, a tandem-rotor compound, and an advancing blade concept configuration. These configurations were deemed, as a first cut, to be technically promising. All the candidate configurations were assessed for the same mission and technology goals and detailed analysis in multiple technology areas was conducted. Extensive engineering analysis was performed, including aircraft design, performance optimization, blade and rotor aerodynamics, airframe aerodynamics, loads and stability analysis, blade structural design, external noise, one-engine inoperative requirements, handling qualities, and cost drivers. This approach was highly successful in attacking this complex design problem.

Design Approach and Analysis Tools

The approach taken was to design large VTOL transports that are economically competitive with today's regional jet airliners and meet the mission and goals. The principal cost drivers are weight, power, and complexity. Advances in structural efficiency, aerodynamic efficiency, control concepts, propulsion concepts, dynamics solutions, and prediction capability should allow substantial reductions in empty weight, power, and fuel. Low power is ensured by low rotor disk loading and low aircraft drag.

The code RC performed the sizing of the rotorcraft, and the comprehensive analysis CAMRAD II was used for performance optimization, and loads and stability calculations. The process is outlined in Figure 2. The sizing code implemented significant weight savings (relative to current technology scaled to large size) as a result of structure, drive train, and engine technology. Cost models were developed, and used to estimate the purchase price and direct operating cost of the heavy-lift rotorcraft designs. The sizing code was used to perform sensitivity analyses, first to optimize the aircraft (variations including disk loading, tip speed, and number of engines), and then to quantify the influence of advanced technology.

The code RC (Ref. 10) was the principal rotorcraft sizing and performance analysis tool for this investigation. RC was developed by the Advanced Design Office of the U. S. Army Aeroflightdynamics Directorate, RDECOM. RC inputs include design strategy (engine sizing, rotor sizing, etc.), rotorcraft parameters (drag coefficients, tail volume ratio, etc.), and requirements and constraints (take-off, payload, range, etc.). RC finds the aircraft that satisfies the designer inputs, then produces the rotorcraft description and conducts the performance analysis (Figure 3).

Technology in the sizing code is introduced in terms of technology factors and performance models. Weights (at the group weight level of detail) are estimated from parametric equations based on historical data. These equations are calibrated to current technology level by comparing with existing aircraft. Technology factors are then applied to represent the impact of advanced technology. In this approach, technology is a change from the statistical equation, attributed to a new configuration or concept, new materials, new design methods, new operating procedures, etc. There are technology factors for blade and hub weight, vibration treatment, drive system weight, and fuselage, wing, and tail weight. Technology also influences performance, in particular rotor hover and cruise efficiency, hub drag, and engine weight and performance.

An assessment of engine and drive train technology was made in order to define and substantiate the sizing code models. The engine model represented what could be obtained from (or required of) modern technology engines.

CAMRAD II is an aeromechanical analysis of helicopters and rotorcraft that incorporates a combination of advanced technologies, including multibody dynamics, nonlinear finite elements, and rotorcraft aerodynamics (Ref. 11). The trim task finds the equilibrium solution (constant or periodic) for a steady state operating condition, and produces the solution for performance, loads, and vibration. The flutter task linearizes the equations about the trim solution, and produces the stability results. The aerodynamic model includes a wake analysis to calculate the rotor nonuniform induced-velocities, using rigid or free wake geometry. CAMRAD II has

undergone extensive correlation with performance and loads measurements on helicopters, tiltrotors, and other rotorcraft configurations. Complete aeroelastic models were developed for each of the configurations considered in this investigation.

The rotor performance model in the RC sizing code was calibrated using the performance calculated by CAMRAD II, and the sizing task repeated. An estimate of the drag of the airframe (based on trends for rotorcraft and turboprop aircraft) was used to define the aerodynamic model for the sizing code and the comprehensive analysis.

CAMRAD II calculations of rotorcraft performance have received extensive correlation with wind tunnel and flight test measurements. Reference 11 presents correlation for several rotorcraft. Reference 12 compares calculations with wind tunnel measurements of the performance of the Tilt Rotor Aeroacoustic Model (TRAM). References 13 and 5 present correlation of calculated rotor performance at high advance ratio with NACA wind tunnel measurements (Ref. 14), XV-1 flight test (Ref. 15), H-34 full scale wind tunnel tests (Ref. 16), and UH-1 full scale wind tunnel tests (Ref. 17). Reference 18 compares calculations of coaxial rotor hover performance for an NACA rotor (Ref. 19), an AFDD model rotor (Ref. 20), and XH-59A flight test (Ref. 21). Correlation has also been performed for forward flight performance correlations with XH-59A flight test data (Ref. 22), in both helicopter and compound configuration.

Cost Models

Cost models were developed for VTOL and CTOL aircraft, based on statistical information for current operations. The cost metrics considered were flyaway cost (purchase price, in 2005 US dollars) and direct operating cost plus interest, DOC+I (in 2005 US cents/ASM). The components of DOC+I were maintenance (airframe, engine, rotor and drive), flight crew, fuel and oil, depreciation, insurance, and finance cost. A principal source for the cost models was Ref. 23 and its unpublished extensions. The CTOL cost model was based on the economics of U. S. airline operations.

In order to compare VTOL and CTOL costs, the two cost models were applied to a Boeing 737-700 at a stage length of 500 miles. For the 737 in the VTOL cost model, the minimum complexity was used, and an installed power trend was used to get an equivalent turboshaft power (Ref. 1). The costs are substantially higher with the VTOL model. With these results it is possible to establish cost technology factors:

Maintenance tech factor = 0.9/9.8 = 0.092
Flyaway price tech factor = 48.0/83.6 = 0.57

The technology factors represent the reduction in VTOL cost needed to match CTOL cost trends, excluding the influence of complexity and the weight and power required for hover operation. Insurance, depreciation, and finance costs are driven by flyaway price. Baseline cost estimates for the heavy-lift rotorcraft designs were obtained using the above cost technology factors. A significant part of the differences between VTOL and CTOL costs must be the very different operations that produced the cost data used to develop the models. The remaining differences in cost must be attacked by advanced technology. Note in particular the importance of maintenance costs, reflected in the large technology factor.

For the same mission, a VTOL aircraft will have higher gross weight and higher installed power than a CTOL aircraft. In addition, there are complexity factors in the VTOL model, including number of rotors and number of blades. Thus there is still a cost of VTOL capability in the model, even when the maintenance and flyaway price technology factors are used.

Mission and Design Conditions

Based on the notional vehicle capabilities and technology goals, the civil mission described in Table 1 was defined. This investigation is not intended to specify the market, but rather to identify enabling technology for civil applications of heavy-lift rotorcraft. Note in particular the OEI requirement: at takeoff conditions (5k ISA+20°C) the contingency power of the remaining engines (133% OEI MCP) must be greater than 90% hover out-of-ground-effect power required (the factor of 90% accounting non-zero speed and some altitude loss during the takeoff).

For maximum utilization, the aircraft must have a wide range of capabilities. Although the aircraft were designed to the mission defined in Table 1, hence with very little hover time, efficient hover and low speed capability is essential to the RIA operational concept. This is reflected in the requirement for essentially OEI hover capability. The resulting designs optimize at balanced cruise and OEI hover power, so the cruise speed of 350 knots can be viewed as a fallout of the OEI requirement. Reasonable downwash and outwash from the rotors hovering in ground effect is required for effective utilization. For example, a download of 20 lb/ft^2 would produce an outwash with a peak velocity of over 90 knots. As a result of these considerations, high disk loading aircraft (such as tiltwings) were not among the configurations considered.

Technology Factors and Design Parameters

Meeting the technology goals requires high speed, high altitude, and long range for productivity. The heavy-lift rotorcraft must have low disk loading for good hover efficiency, and low drag for efficient cruise. The actual disk loadings of the designs were determined based on minimum aircraft weight, power, and cost. For this heavy-lift rotorcraft investigation, the target airframe and wing drag was $D/q = 1.6(W/1000)^{2/3}$. This drag level is higher than current turboprop aircraft, although about 35% lower than is customary in the helicopter industry (Figure 4). So good aerodynamic design practice should be sufficient to achieve the target for airframe drag. For concepts with edgewise rotors in cruise, hub drag must be added to the airframe and wing drag of the aircraft. For this investigation, the target hub drag was $D/q = 0.4(W/1000)^{2/3}$, which is less than half of current hub drag levels (Figure 5). Achieving this hub drag level will require advanced technology, certainly fairings but possibly also active flow control.

The weight technology factors used for the rotorcraft designs are summarized as follows: 79% for rotor blade weight, 96% for rotor hub weight; 67% for drive system weight; 88% for fuselage and wing weight; 90% for empennage weight.

The definition of the technology level in the sizing code also involves performance and aerodynamics. For the rotor, the design blade loading C_W/σ was prescribed, based on an assessment of what advanced technology could provide. Rotor induced and profile power in the sizing code were calibrated to the results of the comprehensive analysis calculations. Thus the sizing code performance represented a rotor with optimum twist, taper, cruise tip speed, etc. However, current technology airfoils were used in the comprehensive analysis optimization. Some further improvement in aircraft performance can thus be expected from the use of advanced technology airfoils, especially if specifically designed for these aircraft. Airframe drag was specified as described above. Current technology values were used for hover download. Some further improvement in aircraft performance might be obtained from download reduction.

The statistical weight equations used in the design code incorporate an influence of aircraft size, based on historical trends. For rotorcraft designed to fixed disk loading, tip speed, blade loading (solidity), and number of blades, these equations imply that rotor blade, rotor hub, and drive system weight scale with gross weight as $W^{1.26}$, $W^{1.39}$, and $W^{1.12}$, respectively. So for an increase in gross weight by a factor of 2.0, the rotor blade, rotor hub, and drive system weight increase by factors of 2.4, 2.6, and 2.2; and the aircraft structural and drive system weight therefore increases by about a factor of 2.2. In order to maintain aircraft empty weight fraction as size increases, the design approach must be changed, which conventionally has resulted in an increase in disk loading with size.

Basic parameters of the rotorcraft were chosen for the heavy-lift configurations based on an assessment of current and future technology. The rotor blade loading (C_W/σ) was chosen considering low speed maneuverability requirements, with about an 8% improvement in maximum lift capability, relative to current technology. A relatively low hover tip speed was used, reflecting the importance of the noise goal. The cruise tip speed was chosen to optimize the performance. Hover download values consistent with current technology were used. A low wing loading was chosen, for good low speed maneuverability and wide conversion speed range. The same blade loading and wing loading design values were used for both tiltrotor and slowed-rotor compound configurations.

Configurations

Three aircraft configurations were the primary subject of the Heavy Lift Rotorcraft Systems Investigation:

1) Large Civil Tiltrotor (LCTR)
2) Large Civil Tandem Compound (LCTC)
3) Large Advancing Blade Concept (LABC)

These configurations were selected by industry as the most promising candidates for the civil mission. The conventional two-rotor tiltrotor configuration was considered, since a quad tiltrotor would not present as much of a challenge in terms of rotor size. A low rotor speed was used for the tiltrotor in cruise, to improve the proprotor propulsive efficiency. The LCTC and LABC use edgewise rotors in cruise, hence the rotor rotation must be slowed as the flight speed increases, in order to keep the advancing tip Mach number reasonable. The LCTC is a slowed-rotor compound: it has a wing and auxiliary propulsion for cruise, so the rotors are operated in an unloaded condition. The LABC uses stiff coaxial main rotors capable of carrying significant roll moment, hence generating lift on the rotor advancing side in forward flight. This configuration has been described as the advancing blade concept, or lift-offset rotors. The LABC requires auxiliary propulsion at high speeds, but has no wing.

The slowed-rotor compound considered had shaft-driven tandem main rotors. Single main rotor and coaxial main rotors are alternate configurations. The number and arrangement of the main rotors affects performance through rotor/rotor and rotor/wing interference; and affects the aircraft size because of antitorque and transmission layout issues. An alternative

to shaft drive is a reaction drive configuration, typically using jets at the blade tips. The reaction drive is used in hover; in cruise the rotor is operated in autorotation. With reaction drive the transmission weight is greatly reduced, but the rotor cruise performance is compromised by the need for thick blades, and the hover performance is poor because of high energy losses entailed in delivering the air to the blade tips.

The heavy-lift rotorcraft designs are summarized in Table 2. Three-views of the aircraft are shown in Figures 6–8. Recall that for these designs the blade loading, hover tip speed, and wing loading were specified, based on assessments of the technology. Cruise tip speed was optimized based on cruise efficiency. The disk loading was optimized, based on aircraft weight, power, and cost. Basically the optimum disk loading produces a balance in power requirement between cruise and OEI hover. Cruise efficiency defines the power available, then the disk loading is chosen that uses that power in hover (a larger rotor would increase the rotor and blade weight, while a smaller rotor would require more power hence more engine and fuel weight). The empty weight fraction is about 65% for all three designs. The fixed weight is comparable to current commercial jet aircraft. The drag of the LCTR is comparable to good turboprop aerodynamic design. The LCTC adds the drag of the hub (less than current technology levels), and the LABC does not have the drag of the wing. This LABC design was produced by the sizing code using a rotor cruise performance that was better than that predicted by the comprehensive analysis.

The aircraft cruise L/D = WV/P (based on cruise power, including losses, at design gross weight) was the principal efficiency metric. For the mission considered, the LCTR has the best cruise efficiency, hence the smallest design gross weight and the smallest installed power (Table 2). Next in efficiency is the LCTC, and after that the LABC.

Figure 9 shows the flyaway cost and DOC+I for the three heavy-lift rotorcraft configurations, and Figure 10 presents the DOC+I breakdown for the 1200 nm design mission. These figures include the Boeing 737 costs for comparison. The block hours per year value was based on Southwest Airlines operations. The difference in dead time between the VTOL and 737 reflected the difference in operations. For the VTOL costs, the aircraft parameters (empty weight, installed power, number of rotors and number of blades) and the mission parameters (fuel weight, block time and block speed for a specified range) were obtained from the RC code.

The VTOL cost model is driven by gross weight and power, so the LCTR has the lowest cost, followed by the LCTC and then the LABC. At the design stage length, the LCTR cost is about 20% higher than that of a current 737. That is the cost of VTOL capability. The LCTR is more economical than the 737 for stage lengths below about 200 miles.

Figure 11 shows the costs for the LCTR with and without the cost technology factors, and Figure 12 presents the corresponding DOC+I breakdown. These results emphasize and quantify the importance of controlling the maintenance costs for heavy-lift rotorcraft.

Assessment of Configurations

The NASA Heavy Lift Rotorcraft Systems Investigation reached the following conclusions (Ref. 1). For the NASA civil mission, the Large Civil Tiltrotor has the best cruise efficiency, hence the lowest weight and lowest cost. The LCTR is the configuration with the most promise to meet the NASA technology goals. The LCTR design presented is economically competitive with comparable fixed wing aircraft, with the potential for substantial impact on the air transportation system. The keys to achieving a competitive aircraft are: low drag airframe and low disk loading rotors; structural weight reduction, for both airframe and rotors; drive system weight reduction; improved engine efficiency; low maintenance design; and manufacturing cost comparable to CTOL aircraft.

The Large Civil Tandem Compound has good cruise efficiency, but less than the tiltrotor, and higher development risk than the tiltrotor. Single main rotor and tandem rotor configurations were comparable in efficiency and risk. Even if reaction drive produces the smallest slowed-rotor compound rotorcraft, the high installed power compromises efficiency, and the reaction drive system has higher noise and substantially increased risk.

The Large Advancing Blade Concept has lower cruise efficiency than the tiltrotor for the NASA civil mission. Lift-offset rotors are much more effective for missions at lower altitudes, as will be illustrated below.

LARGE CIVIL TILTROTOR (LCTR)

The configuration of the Large Civil Tilt Rotor is shown in Figure 6. The aircraft has two tilting rotors at the wing tips, a low wing, non-tilting engines, and a horizontal tail. A quad tiltrotor (two wings and four rotors) would have smaller rotors, but increased complexity and increased aerodynamic interference. The conventional two-rotor tiltrotor configuration is considered here, which allows more exploration of the implications of large size on the rotor system design. A low wing is used for better structural load paths between

wing, airframe, and landing gear. The horizontal tail is sized by trim requirements rather than stability, because the rotors can be used for flight dynamics stabilization as well as control. A vertical tail is not shown, but could be added if needed for yaw trim. A hingeless rotor hub is used. Excessive coning can significantly reduce hover figure of merit, so a tip mass of 1.5 slug was placed on each blade at 95%R. This increases the hover figure of merit by about 2%. Table 2 gives the aircraft characteristics. Performance, loads, and stability calculations were performed. Isolated rotor performance in hover and cruise were calculated using a free wake geometry model. Dynamics characteristics, including rotor and wing structural design and aeroelastic stability calculations, are discussed in Reference 3.

The blade twist and taper were varied to optimize the rotor for hover and cruise performance. The hover condition was 5k ISA+20°C, 650 ft/sec tip speed, C_T/σ = 0.1557. The cruise condition was 350 knots, 30k ISA, 350 ft/sec tip speed, and rotor thrust as required to trim aircraft drag. The twist distribution had two linear segments, inboard (0.0R to 0.5R) and outboard (0.5R to 1.0R). The linear taper ratio was varied while maintaining constant thrust-weighted solidity (constant 75%R chord). Figure 13 presents the results for twist optimization, showing the typical hover-cruise compromise. The performance was calculated for a matrix of inboard and outboard twist values, and Figure 13 shows the envelope of all the points. The result was an optimum twist of –32 deg inboard and –30 deg outboard; and an optimum taper of 0.8 (tip/root chord). This choice emphasizes the cruise condition, because cruise dominates the civil mission considered.

An exploratory investigation was conducted to design airfoils specifically for the hover and cruise operating conditions of the LCTR rotor blades. The resulting airfoil contours are shown in Figure 14, and Figure 15 plots the optimum boundary for twist variations with both state-of-the-art airfoils and these LCTR airfoils.

The rotor performance from the sizing code and the comprehensive analysis are compared in Figures 16 and 17. These results are for current technology rotor airfoils. Figure 16 shows the hover figure of merit of the rotor. Figure 17 shows the cruise rotor propulsive efficiency, and the aircraft equivalent L/D = WV/P. The aircraft L/D = WV/P is 12.45 at the design cruise speed (L/D = WV/P = 11.1 including losses, see Table 2), significantly above current tiltrotor aircraft efficiency. A major contributor to this excellent performance is the use of a low tip speed in cruise (54% of hover tip speed). One consequence of this low tip speed is a very different result for the twist optimization, compared to current designs. Figure 18 shows the influence of the

cruise tip speed on the aircraft design parameters. Two transmission configurations are considered in Figure 18: a 1-speed transmission (engine speed varying with rotor speed), which is the conventional tiltrotor approach; and a 2-speed transmission (engine at optimum speed regardless of rotor speed), with no transmission weight penalty. If the aircraft has a two-speed transmission, so the engine can operate at its optimum speed in both hover and cruise, the improvement in propulsive efficiency as the tip speed is reduced results in significant weight and cost reductions. With a single-speed transmission, the optimum cruise tip speed is only 15% less than the hover tip speed.

TILTROTOR AERODYNAMICS AND INTERFERENCE

To explore further the aerodynamics of tiltrotor aircraft, including wing-rotor interference effects, a tiltrotor was designed to carry a 20-ton payload for 750 miles at 4k/95°F, with a cruise speed of 300 knots (Ref. 4). Figure 19 shows the baseline design, and Table 3 summarizes the aircraft parameters. The gross weight is 146,600 lb. The aircraft has two four-bladed tilting rotors at the wing tips, a high wing, and a horizontal tail. The baseline aircraft design parameters are disk loading of W/A = 15 lb/ft^2, blade loading of C_W/σ = 0.140, and wing loading of W/S = 100 lb/ft^2. The airframe and wing parasite drag is D/q = 55 ft^2. This drag value is considered aggressive in terms of rotorcraft trends but achievable from good fixed wing aerodynamic design practice. A hingeless rotor hub is used. The rotors rotate with the top blades moving outward in airplane mode. A parametric study was conducted to understand the effects of design parameters on the performance of the aircraft.

In addition, a quad tiltrotor was developed (not designed using the RC code) from the baseline conventional tiltrotor, having the same gross weight, disk loading, and airframe size. Figure 20 shows the quad tiltrotor configuration, and Table 3 summarizes the aircraft parameters. The rotor size was determined to maintain the same disk loading as the baseline conventional tiltrotor. The front wing span follows from maintaining the same clearance between the rotor and fuselage, and the front wing chord by maintaining the same aspect ratio as the baseline conventional tiltrotor wing. The rear wing span is 40% larger than the front wing span. The rear wing chord has the same chord as the front wing from the tips to the middle of the semi-span and then linearly increases to the center line. The quarter chord line of the rear wing is kept straight. This design approach results in wing loading of W/S = 67.16 lb/ft^2 for the quad tiltrotor. The rear rotors and wing are located above the front rotors and wing. The rotors

rotate with the top blades moving outward in airplane mode.

Performance calculations were conducted for the design cruise of 300 knots at 4000 ft, 95°F condition. Rotor/rotor, rotor/wing, and wing/wing interferences were accounted for using the vortex wake model. The current analysis does not include fuselage model, which is known to be important for oscillatory interference of the wing on the rotor, but is not usually necessary for wing mean induced drag. No nacelle model was considered, thus any end plating effect was neglected. Typical wake geometries and blade and wing lift distributions for the baseline conventional and quad tiltrotor are shown in Figures 21 and 22 respectively. Only the tip vortices, which dominate the interference, are drawn in these figures, but there was a full vortex lattice behind each blade and wing. The wing wake model consists of a vortex lattice in the near wake behind the wing with 32 aerodynamic panels, rolling up to tip vortices (with shed wake panels between) in the far wake. Thus, comparable models are used for both wing and rotor wakes in this investigation of the interference.

For the conventional tiltrotor, the aircraft was trimmed using elevator, rotor thrust, and pitch attitude to obtain longitudinal and vertical force and pitching moment equilibrium of the aircraft. For some cases, rotor flapping was also trimmed to zero (to reduce loads) using rotor cyclic pitch. For the quad tiltrotor, the aircraft was trimmed using rotor thrust and front and rear wing pitch angles. The rotor thrust was used to achieve longitudinal force equilibrium and the front and rear wing pitch angles were always adjusted so each wing carries half of the gross weight. Rotor flapping was also trimmed to zero using rotor cyclic pitch.

A parametric study was conducted for the conventional tiltrotor, with the objective of understanding the effects of design parameters on the aircraft performance. The following cases were considered.

C1) Change of rotor rotational direction (baseline is top blades outward).

C2) Increase of disk loading to 16.6 lb/ft^2 (reduction of rotor blade radius by 5%). To maintain the same blade loading, blade chord was increased accordingly.

C3) Reduction of cruise tip speed to 350 ft/sec, to increase the propulsive efficiency of the rotor (baseline cruise tip speed is 626 ft/sec).

C4) Reduction of wing angle of attack relative to the fuselage (thus relative to the rotors) by 3 deg, to investigate the effect of lift sharing between rotor and

wing. The aircraft will trim at larger pitch angle, so the rotors will carry more lift.

C5) Increase of wing span by 10%. To maintain the same wing loading, wing chord was reduced accordingly. In this case, the rotors stay at the same wing span as the baseline.

C6) Increase of wing span by 10% (same as C5), but the rotors move to the wing tips with same radius.

C7) Increase of wing span by 10%, rotors move to wing tips, with blade radius increased by 12.2% (maintaining rotor-fuselage clearance; decreasing disk loading to 11.9 lb/ft^2). To maintain the same blade loading, blade chord was decreased accordingly.

Figure 23 shows the performance results in terms of aircraft lift-to-drag ratio L/D = WV/P, calculated without accessory or other losses, all for the design cruise condition of 300 knots. Rotor/rotor and rotor/wing interferences are accounted for using a vortex wake model for both the rotor and the wing, and the performance results with interference effects are compared with those without interference effects. The interference effects changes the aircraft lift-to-drag ratio by up to 2.1% for the parametric variations investigated. The reduction of rotor tip speed (C3) increases the aircraft lift-to-drag ratio the most and the increase of wing span (C5) also has a beneficial effect. The change of rotor rotational direction (C1) decreases the aircraft lift-to-drag ratio significantly and this effect can only be observed with interference included in the calculation. The total effect of changing the rotor direction of rotation was –3.0% of L/D. Rotor disk loading change (C2 compared to baseline, and C7 compared to C6) has a small influence on the aircraft cruise performance. These results are for flapping trimmed to zero; in general, flapping trim does not change the influence of the parameters, but does reduce the aircraft lift-to-drag ratio by up to 1.4% (Ref. 4). The aircraft L/D = WV/P is 7.4 at the design cruise speed (with interference, but without losses), and L/D = WV/P = 7.75 with reduced cruise tip speed (Fig. 23).

Figures 24 and 25 show the show the rotor propulsive efficiency and wing drag (induced and parasite), respectively. These are the same calculations as in Figure 23, except that individual performance components are compared. For the baseline case, there is a significant reduction of the wing induced drag because of the favorable combination of the rotor wake and the wing; and a slight increase in rotor propulsive efficiency because of the nonuniform flow field from the wing interference. The change of rotor rotational direction increases rotor propulsive efficiency somewhat. However, it also increases the wing induced

drag significantly, thus an overall performance penalty is observed. The reduction of rotor tip speed (C3) increases the rotor propulsive efficiency as well as decreases the wing drag. Thus, the most performance improvement is obtained. The tip speed value of 350 ft/sec was selected based on the optimum aircraft performance as shown in Figure 26. The rotor tip speed was varied from 250 to 450 ft/sec and the optimum cruise performance was found at 350 ft/sec tip speed. Further reductions in rotor rotational speed did not improve the aircraft L/D.

The reduction of wing angle of attack (C4) changed lift sharing between the rotor and wing, reducing wing lift by about 4000 lb and increasing rotor lift by about 4000 lb. The reduced wing lift decreases wing induced drag and the increased rotor lift increases rotor induced drag. However, the reduced wing angle of attack also changed wing tip vortex trajectories in such a way as to increase beneficial interference effects, thus the rotor propulsive efficiency was not changed much. The net effect of the reduction of wing angle of attack is a performance improvement. The increase of wing span (C5) decreases the wing drag, but slightly decreases the rotor propulsive efficiency.

Figure 27 illustrates effects of the aerodynamic interference effect on the quad tiltrotor cruise performance. The power required changes due to interference are shown. The interference effects between the front rotors and the front wing and between the rear rotors and the rear wing reduce required power. The front wing has a beneficial influence on the rear rotor power. The rear wing also has a beneficial influence on the front wing (positive interference velocity reduces total induced velocity, and thus reduces wing induced power). The front rotors increase both rear rotor power and rear wing power, although the effect is not significant. A large effect is from the front wing to the rear wing. Much of this wing-wing interference effect is, however, simply the behavior of a tandem-wing configuration, distributing the induced losses between the two wings. It is the substantial deviation from elliptical loading for the combined wing system (see Fig. 22) that produces a non-ideal induced power loss.

Thus aerodynamic interference has a substantial influence on tiltrotor cruise performance, and should be considered in the design optimization. Interference effects improve the aircraft lift-to-drag ratio of the baseline conventional tiltrotor. The interference velocities reduce total induced velocity along the wing span, and thus reduce wing induced power. The interference effect has very small influence on wing profile power and rotor propulsive efficiency. The reduction of rotor tip speed increases the aircraft lift-to-drag ratio the most among the design parameters investigated, and the increase of wing span also has a beneficial effect on the aircraft performance. The change of rotor rotational direction decreases the aircraft lift-to-drag ratio significantly and this effect can only be observed with interference included in the calculation.

LARGE CIVIL TANDEM COMPOUND (LCTC)

The configuration of the Large Civil Tandem Compound is shown in Figure 7. The aircraft has two main rotors in tandem configuration, a high wing, pusher propellers for cruise propulsion, and a horizontal tail. The length of the fuselage follows from the specification of the payload, and the disk loading was optimized to balance the cruise and hover power. As a result there is no overlap of the rotors. The horizontal tail is sized by trim requirements rather than stability. Table 3 gives the aircraft characteristics. Performance, loads, and stability calculations were performed. The comprehensive analysis modelled the auxiliary propulsion as forces applied to the airframe. Rotor/rotor and rotor/wing interference were accounted for using the vortex wake model. A hingeless rotor hub is used.

In hover and low speed flight, standard tandem helicopter controls, plus aircraft pitch and roll attitude, could be used to trim this aircraft. In cruise the aircraft was trimmed using ailerons, elevator, and differential propeller thrust; plus propeller thrust, and aircraft pitch and roll angles. Front and rear rotor collective pitch angles were set to values optimized for cruise performance (optimized rotor thrust). In addition, rotor flapping was trimmed to zero (for load control) using rotor longitudinal and lateral cyclic.

The blade twist and taper were varied to optimize the rotor for hover and cruise performance. The hover condition was 5k ISA+20°C, 650 ft/sec tip speed, C_T/σ = 0.1491. The cruise condition was 350 knots, 30k ISA, 205 ft/sec tip speed, 138764 lb gross weight. The twist distribution had two linear segments, inboard (0.0R to 0.5R) and outboard (0.5R to 1.0R). The linear taper ratio was varied while maintaining constant thrust-weighted solidity (constant 75%R chord). Figure 28 presents the results for twist optimization, showing the hover-cruise compromise. For each value of outboard twist, the inboard twist values are 3, 0, –3, and –6 deg. Figure 29 shows the hover and cruise performance for blades with linear twist, varying from –15 to 0 deg. A large negative twist improves hover performance, but zero twist gives the best cruise performance. The design twist of 0 deg inboard and –12 deg outboard was selected based on the hover-cruise compromise. Compared to –9 deg linear twist, this choice gives 0.3%

8

better hover performance and 1.6% better cruise performance.

The results for blade taper variation are shown in Figure 30. Although the taper of 1.0 produced the best aircraft L/D, the taper of 0.8 (tip/root chord) was selected to reduce blade weight.

The rotor advancing tip Mach number was varied from 0.7 to 0.9 to find the optimum rotor rotational speed for high speed cruise flight, as shown in figure 31. To maintain low rotor drag at high speed, it is necessary to slow the rotor. The optimum cruise performance is found at M_{at} = 0.80 (for the airfoils used). Further reductions in rotor rotational speed do not improve the aircraft L/D.

Performance results from the comprehensive analysis are shown in Figures 32 and 33. These results are for state-of-the-art rotor airfoils. The optimized design has a twist of 0 deg inboard (0.0R to 0.5R) and –12 deg outboard (0.5R to 1.0R), collective angle of -2 deg, and a taper of 0.8 (tip/root chord). The hover figure of merit of an isolated rotor is calculated for the 5k/ISA+20°C condition, with 650 ft/sec tip speed. The results are shown in Figure 32. The calculation was conducted using nonuniform inflow with a free wake geometry. The figure of merit increases as the thrust increases up to around C_T/σ = 0.18, and then decreases. The figure of merit is around 0.73 at the design thrust (C_T/σ = 0.149).

Figure 33 shows the aircraft lift-to-drag ratio at 30,000 ft. The calculation was conducted using nonuniform inflow with a prescribed wake geometry. Rotor/rotor and rotor/wing interference were included in the comprehensive analysis model. The speed varies from 250 to 450 knots; with the rotor tip speed decreasing from hover to cruise speed (350 knots) in order to maintain M_{at} = 0.8 and then 205 ft/sec tip speed was maintained up to 450 knots. The rotor performance in cruise is presented in terms of aircraft L/D = WV/P, calculated without accessory or other losses, and using a propeller efficiency of 0.86 (from the sizing code). The aircraft lift-to-drag ratio decreases as speed goes up. At the design cruise speed, the aircraft lift-to-drag ratio is L/D = WV/P = 10.1 (9.3 including losses, see Table 2).

The maximum hover figure of merit of the compound tandem rotor occurs at around C_T/σ = 0.17 (Fig. 32), which is high compared with many conventional helicopter rotors. The figure of merit for a conventional articulated rotor was calculated and compared with that of the compound tandem rotor, as shown in Figure 34. The conventional rotor has 7 blades, existing airfoils, and typical solidity, twist, tip speed. The maximum figure of merit of the conventional rotor occurs at low

blade loading and the figure of merit value decreases as the blade loading increases. A parametric study was conducted to examine the differences in the figure of merit trend. The parameters investigated in this study are twist, taper, tip speed, and airfoils. The effects of those parameters on the prediction of hover figure of merit were examined by replacing the compound tandem rotor quantities with the conventional rotor quantities. Figure 34 shows the parametric study results. The twist, taper, and tip speed increases the figure of merit at low blade loading, but decreases it at high blade loading. The biggest influence comes from the airfoil change. A significant reduction of the hover figure of merit is observed at high blade loading and the trend becomes similar to the conventional rotor. It appears that the state-of-the-art airfoils used for the compound tandem rotor design have a strong influence on the figure of merit trend.

COMPOUND HELICOPTER

To explore further the aerodynamics of compound helicopters, a design and aeromechanics investigation was conducted for a 100,000 lb compound helicopter with a single main rotor, which is to cruise at 250 knots at 4k/95°F (Ref. 5). This aircraft was sized based on the basic design parameters (not using the RC code). Figure 35 shows the configuration, and Table 4 gives the basic aircraft parameters. The aircraft has a six-bladed rotor, a high wing, a horizontal tail, and two auxiliary propellers located on the wing for cruise propulsion and anti-torque in hover. State-of-the-art rotor airfoils are used for the main rotor blades. A hingeless rotor hub is used. Blade inertial and structural properties are scaled from the LCTC blade.

The baseline aircraft design parameters are disk loading of W/A = 15 lb/ft², blade loading of C_T/σ = 0.14, and wing loading of W/S = 100 lb/ft². These values are from the optimum design for the LCTC, and is shown below to give good performance for the present aircraft. The C_T/σ = 0.14 and W/S = 100 are appropriate for an aircraft that unloads the rotor at a relatively low speed. The aircraft parasite drag is D/q = 40.5 ft². This drag value, which was obtained from historic trends (Fig. 4), is higher than current turboprop aircraft, but lower than is customary in the helicopter industry. The baseline design has a wing span equal to the rotor diameter (Fig. 35). The hover tip speed is 750 ft/sec, and the cruise tip speed of 502 ft/sec which gives M_{at} = 0.8 at 250 knots. The advance ratio is then V/V_{tip} = 0.84 at 250 knots.

A parametric study of key rotor design parameters was conducted with the comprehensive analysis. The baseline design has disk loading of 15, design blade loading of 0.14, wing loading of 100, collective angle of 0 deg, and shaft angle of attack of 3 deg. The blade twist

was varied to obtain balanced hover and cruise performance. The hover condition was 750 ft/sec tip speed, $C_T/\sigma = 0.1484$ (assumed 6% download). The cruise condition was 250 knots, 502 ft/sec tip speed. The twist distribution had two linear segments, inboard (0.0R to 0.5R) and outboard (0.5R to 1.0R). Figure 36 presents the results for twist variation. For each value of outboard twist, the inboard twist values are −3, 0, 3, and 6 deg. A large negative twist improves hover performance, but the zero twist gives the best cruise performance. The design twist of 0 deg inboard and −12 deg outboard was selected based on the hover-cruise compromise. The aircraft lift-to-drag ratio the hover figure of merit variations in Figure 36 are larger than those for the LCTC (Fig. 28). Thus, the blade twist is a more important parameter for the current design than for the LCTC. However, the aircraft lift-to-drag is less sensitive to the inboard twist change for fixed outboard twist. Thus, the benefit of bi-linear twist diminished for the current design compared with the LCTC.

The blade taper ratio was varied as shown in Figure 37. The linear taper ratio was varied while maintaining constant thrust-weighted solidity (chord at 75%R). Although the taper of 1.0 produced the best aircraft lift-to-drag ratio, the taper of 0.8 (tip/root chord) was selected to reduce the blade weight.

The rotor advancing tip Mach number was varied from 0.5 to 0.9 to investigate the effects of the rotor rotational speed on the cruise performance, as shown in Figure 38. It should be noted that the rotor advancing tip Mach number in cruise would be 1.02 with the hover tip speed. To maintain low rotor drag at high speed, it is necessary to slow the rotor. The aircraft lift-to-drag ratio increases as the advancing tip Mach number decreases, reaching the maximum at $M_{at} = 0.55$, which corresponds to $V/V_{tip} = 1.98$. Most of the benefit of slowing the rotor occurs at the initial 20 to 30% reduction of the advancing blade tip Mach number. The design point was selected at $M_{at} = 0.80$, which corresponds to $V/V_{tip} = 0.84$. This values corresponds to about 20% reduction of the advancing blade tip Mach number and 33% reduction of the rotor tip speed from hover condition.

Performance results for the baseline aircraft are shown in Figures 39 and 40. The hover figure of merit of an isolated rotor is calculated with 750 ft/sec tip speed and the result is shown in Figure 39. The calculation was conducted using nonuniform inflow with free wake geometry. The figure of merit decreases as the thrust increases. The figure of merit is around 0.78 at the design thrust ($C_T/\sigma = 0.1484$ with assumed 6% hover download). Figure 40 shows the aircraft lift-to-drag ratio with different airspeeds. The calculation was conducted using nonuniform inflow with prescribed wake geometry. The airspeed varies from 200 to 350 knots, with the rotor tip speed linearly decreased from hover. The aircraft lift-to-drag ratio decreases as airspeed goes up. At the design cruise speed (250 knots), the aircraft lift-to-drag ratio is L/D = WV/P = 7.69 (without losses).

Design variations of wing loading (W/S = 100 vs. 120), blade loading ($C_T/\sigma = 0.14$ vs. 0.09), and disk loading (W/A = 15 vs. 12) were examined. The larger disk area will give lower hover power. The larger blade area or smaller wing area correspond to loading the rotor rather than the wing. Note that $C_T/\sigma = 0.09$ would be appropriate for an advanced technology helicopter, hence the rotor could carry the aircraft weight to conventional helicopter speeds. Figures 41 through 45 show the performance results in terms of aircraft lift-to-drag ratio L/D = WV/P, calculated without accessory or other losses, and using a propeller efficiency of 0.86, all for the design cruise condition of 250 knots. For each combination of disk loading, design blade loading, and wing loading, three collective angles (−3, 0, and 3 deg) and six values for the difference between wing incidence and shaft tilt angle ($\alpha_w - \alpha_s = -4, -1, 1, 3, 5,$ and 7 deg) are shown. The collective and incidence angle variations change the lift share between the rotor and the wing. The rotor speed was that required for $M_{at} = 0.8$. Figure 41 shows the effect of wing loading (W/S = 100 vs. 120) on aircraft lift-to-drag ratio for W/A = 15 and $C_T/\sigma = 0.14$. To obtain higher wing loading, wing area was reduced by decreasing wing span with fixed chord. The aircraft lift-to-drag ratio increases as $\alpha_w - \alpha_s$ increases (wing incidence increases or rotor shaft tilts forward) up to 3 deg for the collective angle of 0 and −3 deg and up to 5 deg for the collective angle of 3 deg, and then decreases. The best performance was obtained for the collective angle of 0 or −3 deg and $\alpha_w - \alpha_s = 3$ deg. Lower wing loading (higher wing area) increased the aircraft lift-to-drag ratio. The smaller wing area corresponds to loading the rotor rather than the wing. A wing is a more efficient lifting device than a rotor for the current 250 knot compound helicopter, thus the larger wing area improves the aircraft performance.

Figure 42 shows the effect of blade loading ($C_T/\sigma = 0.14$ vs. 0.09) on aircraft lift-to-drag ratio for W/A = 15 and W/S = 100. To obtain lower blade loading, blade area was increased by increasing blade chord for a given blade radius. Thus, solidity was increased but aspect ratio was decreased. The larger blade area corresponds to loading the rotor rather than the wing. Higher design blade loading (smaller blade chord) increased the aircraft lift-to-drag ratio because the smaller blade chord reduced rotor profile power.

Figure 43 shows the effect of disk loading (W/A = 15 vs. 12) on aircraft lift-to-drag ratio for W/S = 100 and C_T/σ = 0.14. To obtain lower disk loading, rotor diameter was increased, but to maintain the same blade loading for the increased rotor diameter, blade chord was decreased. Thus, the blade areas are identical for the two cases. Disk loading has a small influence on the aircraft performance, although it will have an impact on hover performance and the rotor weight.

The optimum required rotor shaft power and optimum lift sharing between the rotor and wing are shown in Figures 44 and 45 for the baseline aircraft (W/A = 15, C_T/σ = 0.14, W/S = 100) at cruise speed of 250 knots. Figure 44 shows the rotor shaft power for the baseline aircraft. The rotor power increases as α_w–α_s increases. At the optimum aircraft lift-to-drag ratio, the rotor shaft power is a small positive value: between 500 and 1000 hp. With the rotor in autorotation (zero rotor shaft power), the rotor thrust is large, hence the total rotor drag larger and the aircraft L/D somewhat smaller. Figure 45 shows the rotor and wing lift for the baseline aircraft. As α_w–α_s increases, the rotor lift decreases and wing lift increases. A higher collective angle increases rotor lift and decreases wing lift. At the optimum lift sharing between the rotor and wing, the rotor carries 8-9% of the aircraft gross weight. The optimum lift sharing between the rotor and wing varies with disk loading, design blade loading, and wing loading.

LIFT-OFFSET COAXIAL HELICOPTER

The lift-offset or advancing blade concept helicopter has the potential to achieve high-speed cruise with the rotor carrying the aircraft lift. The lift-offset rotor uses stiff blades capable of carrying significant hub roll moments, hence generating lift on the rotor advancing side in forward flight. This configuration still requires auxiliary propulsion, but does not need to unload the aircraft weight onto a wing in cruise. A 150,000 lb helicopter utilizing coaxial lift-offset rotors was investigated, with a design cruise speed of 250 knots at 5k/ISA+20°C. This aircraft was sized based on the basic design parameters (not using the RC code). Figure 46 shows the configuration, and Table 4 gives the aircraft parameters. The aircraft has coaxial four-bladed rotors. A small wing is required to support the auxiliary propulsion (likely propellers), and hence can carry some lift in cruise. Lift-offset rotors require a hingeless rotor hub, in order to carry the hub moment. Blade inertial and structural properties are scaled from the LABC blade (Ref. 1).

The baseline aircraft design parameters are disk loading of W/A = 15 lb/ft^{2}, blade loading of C_T/σ = 0.10, and maximum advancing tip Mach number of M_{at} = 0.9. The design operating condition was 5k/ISA+20°C, for both hover and 250 knots. The choice of these parameters was based on the LABC optimization (Ref. 1), with the lower design altitude appropriate for a lift-offset rotor. The design lift offset is M/LR = 0.25 (rotor hub roll moment M, divided by rotor lift times rotor radius LR). The rotor vertical separation is 6% of the diameter. Advanced technology rotor airfoils are assumed for the main rotor blades, permitting M_{at} = 0.9 as well as achieving a mean blade drag coefficient of c_{do} = 0.0090 in both hover and cruise. The hover tip speed is 700 ft/sec, and the cruise tip speed is 600 ft/sec, which gives M_{at} = 0.9 and an advance ratio of V/V_{tip} = 0.70 at 250 knots.

The wing is sized to carry 20% of the weight at the cruise condition, with a wing loading of W/S = 120 lb/ft^{2}. The resulting wing lift coefficient is 0.7. The aircraft parasite drag is D/q = 50.0 ft[2]. This drag value is aggressive for a rotorcraft, and would probably require flow control for hub drag reduction. The power was calculated using a propeller efficiency of 0.90 for the auxiliary propulsion. These values for the airfoil drag, airframe drag, and propulsive efficiency are aggressive, hence the calculated aircraft cruise performance is somewhat optimistic.

The blade twist was varied to obtain balanced hover and cruise performance. The hover condition was 700 ft/sec tip speed, C_T/σ = 0.0919. The cruise condition was 250 knots, 600 ft/sec tip speed. The twist distribution has four linear segments, with breaks at 0.25R, 0.50R, and 0.75R. Figure 47 presents the results for twist variation. The optimum twist is –3/–6/–15/–18 deg (inboard to outboard, equivalent root-to-tip linear rate). The performance is much more sensitive to the outboard twist (varied in Fig. 47) than to the inboard twist. In Figure 47, the twist of the last segment (0.75R to 1.00R) has values from –12 to –24 deg; the lines are for the twist of the third segment (0.50R to 0.75R) being equal to that of the last segment, –3 deg more, or –6 deg more. The optimum is a compromise between cruise and hover.

The blade taper ratio was varied as shown in Figure 48. As for twist, four segments are used with linear taper in each. The optimum taper was 1.333/1.333/1.333/ 0.333 (effective tip/root chord ratio). The performance is much more sensitive to the outboard taper than to the inboard taper. In Figure 48, the taper of the last segment has values of 0.667, 0.5, and 0.333; for several values of the taper in the third segment.

Performance results for the lift-offset aircraft are shown in Figures 49 and 50. Figure 49 shows the rotor effective lift-to-drag ratio (L/D_e = TV/(P_i+P_o), from rotor induced and profile power) as a function of airspeed, for several values of the rotor lift offset.

Figure 50 shows the corresponding aircraft L/D = WV/P, calculated without accessory or other losses, and using a propeller efficiency of 0.90. The calculation was conducted using nonuniform inflow with prescribed wake geometry. The airspeed varies from 100 to 280 knots, with the rotor tip speed varying to keep the advancing tip Mach number below or at M_{at} = 0.90, and the wing lift coefficient fixed. At the design cruise speed (250 knots), the rotor effective L/D_e is 10.4 and the aircraft lift-to-drag ratio is L/D = WV/P = 6.2. Lift-offset is effective above 200 knots.

CONCLUSION

NASA and the U.S. Army at Ames Research Center are conducting investigations of the aerodynamic performance capability of rotorcraft designed for heavy-lift and high-speed cruise. The NASA Heavy Lift Rotorcraft Systems Investigation examined in depth several rotorcraft configurations for large civil transport, designed to meet the technology goals of the NASA aeronautics program. Further explorations have been conducted of the performance of tiltrotor, compound helicopter, and lift-offset rotor configurations, for both military and civil missions.

These investigations have shown that heavy-lift, high-speed, long-range rotorcraft can be designed that are economically competitive and operationally effective, with the potential for substantial impact on both civil and military air transportation systems. Table 5 summarizes the calculated cruise performance of the configurations examined.

This work continues, including exploration of additional design conditions and multi-mission requirements, further refinement and optimization of the designs, application of higher-fidelity aeromechanics analyses to the configurations, and closer coupling of the sizing code to the resulting performance calculations.

REFERENCES

[1] Johnson, W.; Yamauchi, G.K.; and Watts, M.E. "NASA Heavy Lift Rotorcraft System Investigation." NASA TP 2005-213467, December 2005.

[2] Johnson, W.; Yamauchi, G.K.; and Watts, M.E. "Design and Technology Requirements for Civil Heavy Lift Rotorcraft." American Helicopter Society Vertical Lift Aircraft Design Conference, San Francisco, CA, January 2006.

[3] Acree, C.W., Jr., and Johnson, W. "Performance, Loads and Stability of Heavy Lift Tiltrotors." American Helicopter Society Vertical Lift Aircraft Design Conference, San Francisco, CA, January 2006.

[4] Yeo, H., and Johnson, W. "Aeromechanics Analysis of a Heavy Lift Slowed-Rotor Compound Helicopter." *Journal of Aircraft*, Vol. 44, No. 2, pp. 501-508, March-April 2007.

[5] Yeo, H., and Johnson, W. "Optimum Design of a Compound Helicopter." HeliJapan 2006, AHS International Meeting on Advanced Rotorcraft Technology and Life Saving Activities, Nagoya, Japan, November 2006.

[6] Yeo, H., and Johnson, W. "Performance and Design Investigation of Heavy Lift Tiltrotor with Aerodynamic Interference Effects." American Helicopter Society 63rd Annual Forum, Virginia Beach, VA, May 2007.

[7] Johnson, J., Stouffer, V., Long, D., and Gribko, J., "Evaluation of the National Throughput Benefits of the Civil Tiltrotor," NASA CR 2001-211055, September 2001.

[8] Stouffer, V., Johnson, J., and Gribko, J., "Civil Tiltrotor Feasibility Study for the New York and Washington Terminal Areas," NASA CR 2001-210659, January 2001.

[9] Smith, D. E., Wilkerson, J., Montoro, G. J., Coy, J., and Zuk, J., "Technology Development for Runway Independent Aircraft," American Helicopter Society 59th Annual Forum, Phoenix, AZ, May 2003.

[10] Preston, J., and Peyran, R., "Linking a Solid-Modeling Capability with a Conceptual Rotorcraft Sizing Code," American Helicopter Society Vertical Lift Aircraft Design Conference, San Francisco, CA, January 2000.

[11] Johnson, W., "Rotorcraft Aeromechanics Applications of a Comprehensive Analysis," HeliJapan 98: AHS International Meeting on Advanced Rotorcraft Technology and Disaster Relief, Gifu, Japan, April 1998.

[12] Johnson, W. "Calculation of Tilt Rotor Aeroacoustic Model (TRAM DNW) Performance, Airloads, and Structural Loads." American Helicopter Society Aeromechanics Specialists's Meeting, Atlanta, GA, November 2000.

[13] Floros, M.W., and Johnson, W. "Performance Analysis of the Slowed-Rotor Compound Helicopter Configuration." American Helicopter Society 4th Decennial Specialists' Conference on Aeromechanics, San Francisco, CA, January 2004.

[14] Jenkins, J.L., Jr. "Wind-Tunnel Investigation of a Lifting Rotor Operating at Tip-Speed Ratios from 0.65 to 1.45." NASA TN D-2628, February 1965.

[15] Hohenemser, K. H., "Full Scale Rotor Tests of the Air Force Convertiplane Model XV-1 in the NACA 40

x 80 Foot Wind Tunnel at Moffett Field, California." McDonnell Aircraft Report 3379, McDonnell Aircraft Corporation, February 1954.

[16] McCloud, J.L.; Biggers, J.C.; and Stroub, R.H. "An Investigation of Full-Scale Helicopter Rotors at High Advance Ratios and Advancing Tip Mach Numbers." NASA TN D-4632, July 1968.

[17] Charles, B.D., and Tanner, W.H., "Wind Tunnel Investigation of Semirigid Full-Scale Rotors Operating at High Advance Ratios," USAAVLABS TR 69-2, January 1969.

[18] Lim, J.W.; McAlister, K.W.; and Johnson, W. "Hover Performance Correlation for Full-Scale and Model-Scale Coaxial Rotors." American Helicopter Society 63rd Annual Forum, Virginia Beach, VA, May 2007.

[19] Harrington, R.D., "Full-Scale-Tunnel Investigation of the Static-Thrust Performance of a Coaxial Helicopter Rotor," NACA TN 2318, 1951.

[20] McAlister, K.W.; Tung, C.; Rand, O.; Khromov, V.; and Wilson, J. S., "Experimental and Numerical Study of a Model Coaxial Rotor." American Helicopter Society 62nd Annual Forum, Phoenix, AZ, May 2006.

[21] Arents, D.N., "An Assessment of the Hover Performance of the XH-59A Advancing Blade Concept Demonstration Helicopter," Report USAAMRDL-TN-25, May 1977.

[22] Ruddell, A.J., et al. "Advancing Blade Concept (ABC) Technology Demonstrator." USAAVRADCIM TR 81-D-5, April 1981.

[23] Harris, F.D., and Scully, M.P., "Rotorcraft Cost Too Much." *Journal of the American Helicopter Society*, Vol. 43, No. 1, January 1998. (Additionally, Harris, F.D. "An Economic Model of U.S. Airline Operating Expenses," unpublished.)

NOMENCLATURE

A	rotor disk area
c_{do}	mean drag coefficient for profile power
C_T	rotor thrust coefficient, $T/(\rho A V^2_{tip})$
C_W	rotor weight coefficient, $W/(\rho A V^2_{tip})$
D/q	airframe drag divided by dynamic pressure
FM	rotor hover figure of merit, $(T\sqrt{(T/2\rho A)})/P$
L/D	aircraft effective lift-to-drag ratio, WV/P (based on cruise power)
L/D_e	rotor effective lift-to-drag ratio, $TV/(P_i+P_o)$ (based on rotor induced and profile power)
M_{at}	advancing tip Mach number
P	aircraft power
R	rotor radius
T	rotor thrust
V	flight speed
V_{tip}	rotor tip speed
W	gross weight
W/A	disk loading
W/S	wing loading
α_s	rotor shaft angle (positive aft)
α_w	wing incidence angle
η	propeller efficiency, TV/P
ρ	air density
σ	rotor solidity (ratio blade area to disk area)
ASM	available seat miles
CTOL	conventional takeoff and landing
DOC+I	direct operating cost plus interest
ISA	international standard atmosphere
LABC	Large Advancing Blade Concept
LCTC	Large Civil Tandem Compound
LCTR	Large Civil Tilt Rotor
MCP	maximum continuous power
MRP	maximum rated power
OEI	one-engine inoperative
OGE	out of ground effect
RC	AFDD design code
RIA	runway independent aircraft
VTOL	vertical takeoff and landing

Table 1. Civil design mission.

    1200 nm range, 120 passengers (26400 lb payload)
    Cruise at 350 knots and 30000 ft (min 22000 ft, for icing)
    Design mission
            Idle 5 min
            Takeoff + 1 min Hover OGE   5k ISA+20°C
            [convert]
            Climb at V best range (0k ISA to 30k ISA, distance part of range)
            Cruise at 350 knots, for 1200nm range   30k ISA
            Reserve: 30 min + 30 nm at V-best-range   30k ISA
            Descend at V-best-range (no range credit)
            [convert]
            1 min Hover OGE + Landing   5k ISA+20°C
            Idle 5 min
    Design power
            Hover: 95% MRP, 5k ISA+20°C
            Cruise: 100% MCP, 30k ISA
            One engine inoperative (OEI):
                    at 5k ISA+20°C, 133% (OEI MCP) greater than 90% (Hover OGE P required)
                    at 22k ISA, (OEI MCP) greater than (P required at V-best-range)
                    4 engines

Table 5. Summary of calculated aircraft cruise performance.

Aircraft	cruise condition	$(D/q)/(W/1000)^{2/3}$	prop η	L/D=WV/P
Large Civil Tiltrotor (LCTR)	350 kts, 30k	1.50		12.45
Tiltrotor	300 kts, 4k 95°F	1.98		7.4
Tiltrotor (reduced rotor speed)	300 kts, 4k 95°F	1.98		7.75
Large Civil Tandem Compound (LCTC)	350 kts, 30k	1.88	0.86	10.1
Compound helicopter	250 kts, 4k 95°F	1.88	0.86	7.7
Lift-offset coaxial helicopter	250 kts, 5k ISA+20°C	1.77	0.90	6.2

Table 2. Heavy-lift rotorcraft designs.

	LCTR	LCTC	LABC
	tiltrotor	tandem compound	advancing blade
Mission gross weight (lb)	123562	138764	160636
Engines (hp)	4x6914	4x9684	4x14267
Rotor diameter (ft)	88.7	76.7	90.5
Disk loading W/A (lb/ft^2)	10	15	25
C_W/σ (geom, 5k ISA+20°C)	0.133	0.133	0.0675
C_W/σ (T-wt, 5k ISA+20°C)	0.141	0.141	0.090
Hover tip speed (ft/sec)	650	650	650
Cruise tip speed (ft/sec)	350	205	255
maximum M_{at}	0.70	0.80	0.85
V/V_{tip}	1.69	2.88	2.32
Solidity	0.0881	0.1321	0.1721
Number blades per rotor	4	4	5
chord (75%R, ft)	3.06	3.98	4.89
aspect ratio	14.5	9.6	9.2
taper ratio	0.8	0.8	0.33
Drag D/q (ft^2)	37.3	50.3	38.1
(D/q)/(W/1000)$^{2/3}$	1.50	1.88	1.29
body-interference-tail D/q	13.2	14.4	15.1
pylon D/q	10.0	9.4	9.5
wing D/q	14.1	15.8	–
hub D/q	–	10.7	13.5
hub (D/q)/(W/1000)$^{2/3}$	–	0.40	0.45
Wing loading (lb/ft^2)	80	80	–
area (ft^2)	1545	1735	–
span (ft)	105	144	–
Aspect ratio	7.1	12.0	–
Weight empty fraction	65.3%	65.6%	64.7%
Lock number	12.1	13.0	19.1
Total blade weight (lb), all rotors	5960	5168	10800
Mission, payload	120 pass	120 pass	120 pass
range (nm)	1200	1200	1200
cruise altitude (ft)	30000	30000	30000
cruise speed (kt)	350	350	350
Cruise power (hp)	11904	15956	25068
Cruise L/D = WV/P	11.1	9.3	6.9
Cruise prop η / rotor D/q / rotor L/D$_e$	0.81	16.7	7.7 †
Hover figure of merit (5k ISA+20°C)	0.78	0.73	0.68 †

† sizing code used hover figure of merit = 0.79, cruise L/D$_e$ = 12.0

Table 3. Characteristics of baseline tiltrotor and quad tiltrotor designs.

	Tiltrotor	Quad Tiltrotor
	RC designed	developed from tiltrotor
Mission gross weight (lb)	146600	146600
Engines (hp)	2x18710	
Rotor diameter (ft)	78.9	55.8
Disk loading W/A (lb/ft^2)	15	15
C_W/σ (geom, 4k/95°F)	0.140	0.140
C_W/σ (T-wt, 4k/95°F)	0.154	0.154
Hover tip speed (ft/sec)	750	750
Cruise tip speed (ft/sec)	626	626
Solidity	0.0989	0.0989
Number blades per rotor	4	4
chord (75%R, ft)	2.79	1.97
taper ratio	0.7	0.7
Drag D/q (ft^2)	55.0	60.3
(D/q)/(W/1000)$^{2/3}$	1.98	2.17
Wing loading (lb/ft^2)	100	67.2
area (ft^2)	1466	848 (front) & 1335 (rear) = 2183
span (ft)	96.4	73.3 (front) & 102.6 (rear)
Mission, payload	20 ton	
range (nm)	750	
cruise altitude (ft)	4000, 95°F	
cruise speed (kt)	300	

Table 4. Characteristics of compound helicopter and lift-offset coaxial helicopter designs.

	Compound Helicopter	Lift-Offset Coaxial Helicopter
	developed from parameters	developed from parameters
Mission gross weight (lb)	100000	150000
Rotor diameter (ft)	92.1	112.8
Disk loading W/A (lb/ft^2)	15	15
C_W/σ (geom, 4k/95°F)	0.140	
C_W/σ (T-wt, 4k/95°F)	0.148	0.100
Hover tip speed (ft/sec)	750	700
Cruise tip speed (ft/sec)	502	600
Solidity	0.0992	0.0871 (per rotor)
Number blades per rotor	6	4
chord (75%R, ft)	2.39	3.86
taper ratio	0.8	1.333/0.333
Drag D/q (ft^2)	40.5	50.0
(D/q)/(W/1000)$^{2/3}$	1.88	1.77
Wing loading (lb/ft^2)	100	120
area (ft^2)	1000	250
span (ft)	92.1	38.7
Mission, payload		
range (nm)		
cruise altitude (ft)	4000, 95°F	5k ISA+20°C
cruise speed (kt)	250	250

Figure 1. Runway Independent Aircraft (RIA) industry concepts from 2002: Sikorsky Reverse Velocity Rotor (top), Boeing Tiltrotor (center), Bell Quad Tiltrotor (bottom).
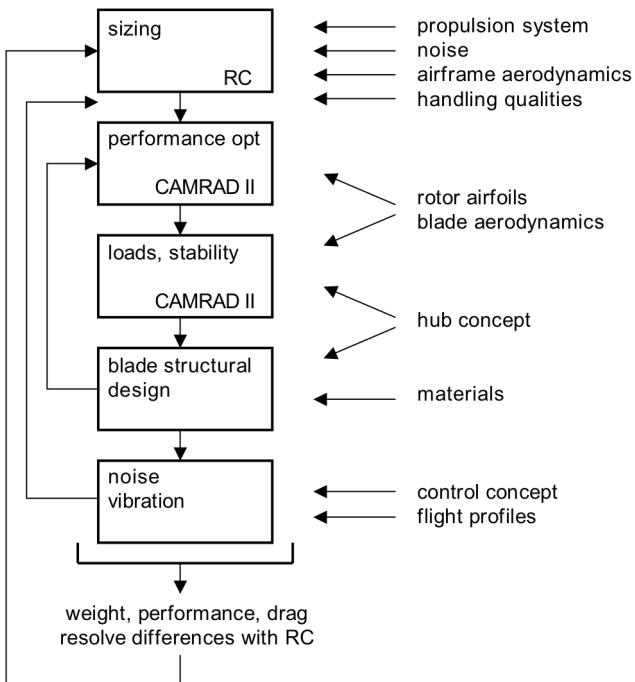
Figure 2. Outline of iterative design process.
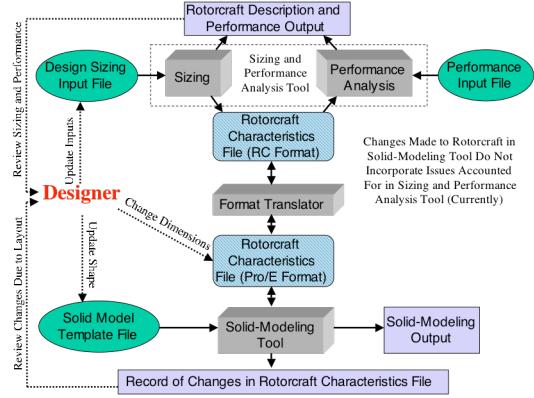
Figure 3. Simplified conceptual design process.
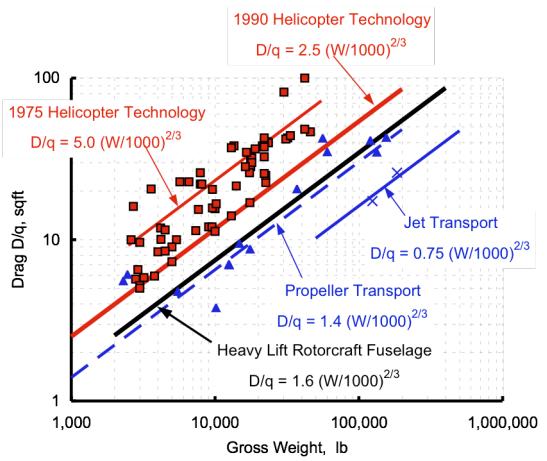
Figure 4. Aircraft drag trends (courtesy F.D. Harris).
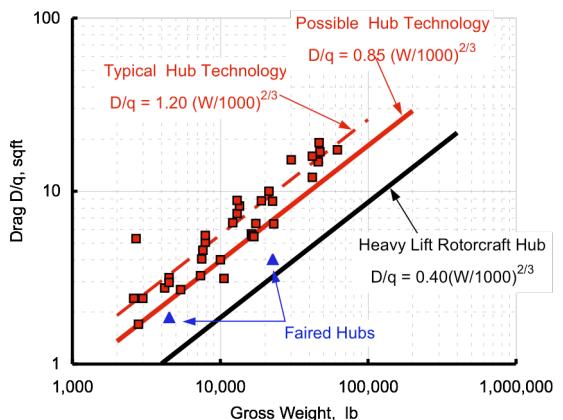
Figure 5. Helicopter hub drag trends (courtesy F.D. Harris).
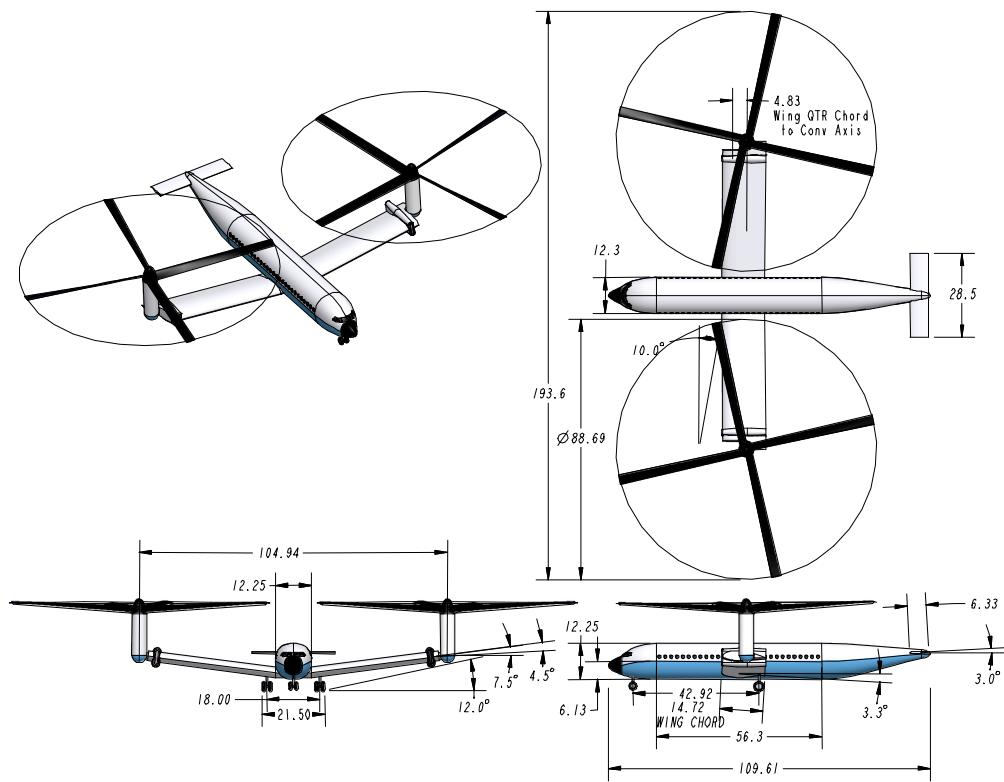
Figure 6. Three-view of Large Civil Tiltrotor (LCTR).
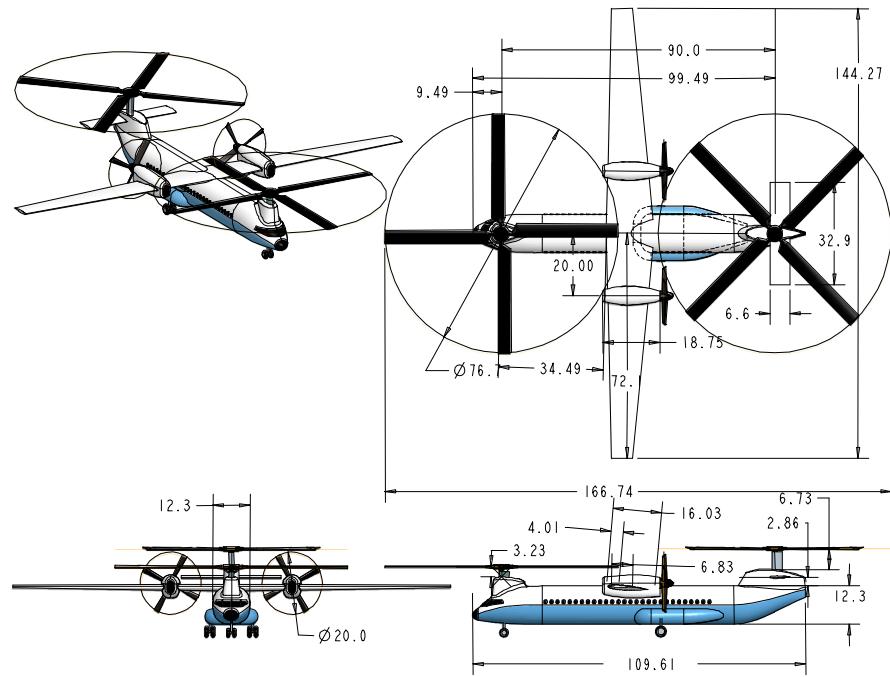
Figure 7. Three-view of Large Civil Tandem Compound (LCTC).
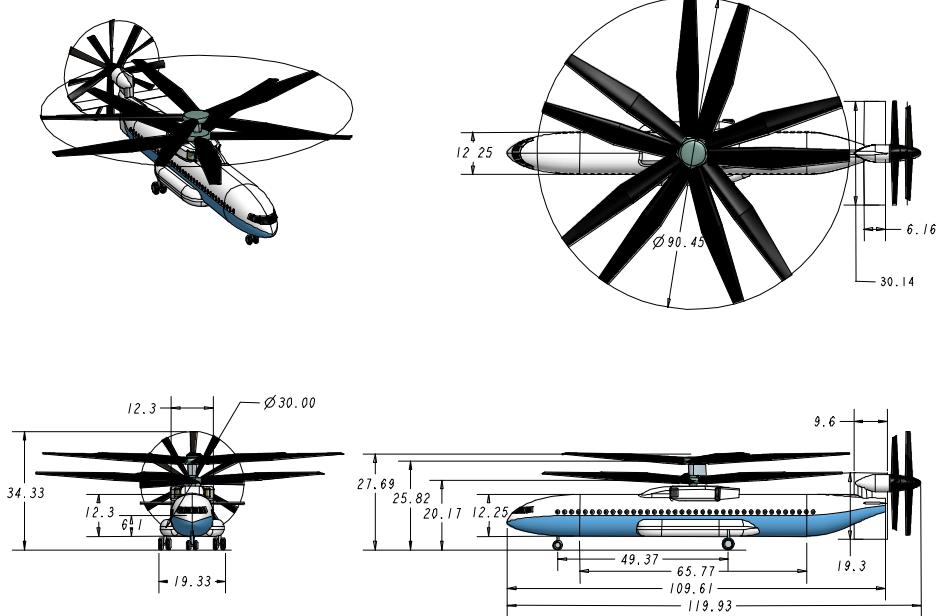
Figure 8. Three-view of Large Advancing Blade Concept (LABC)
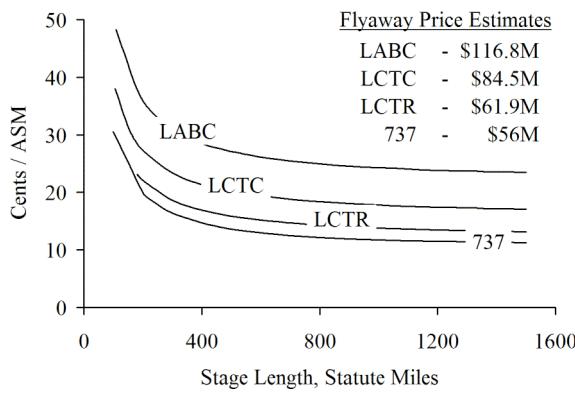
Figure 9. Flyaway price (2005 USD) and DOC+I (2005 cents/ASM) comparisons for baseline designs.
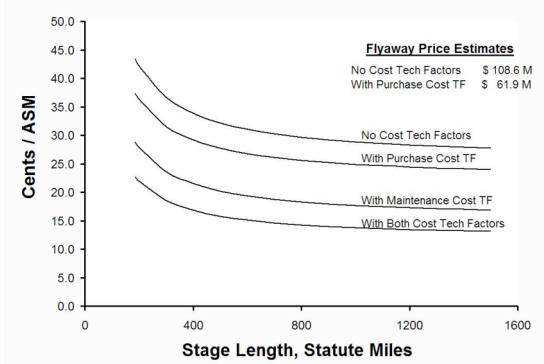
Figure 11. Effect of cost technology factors on flyaway price (2005 USD) and DOC+I (2005 cents/ASM) for LCTR.
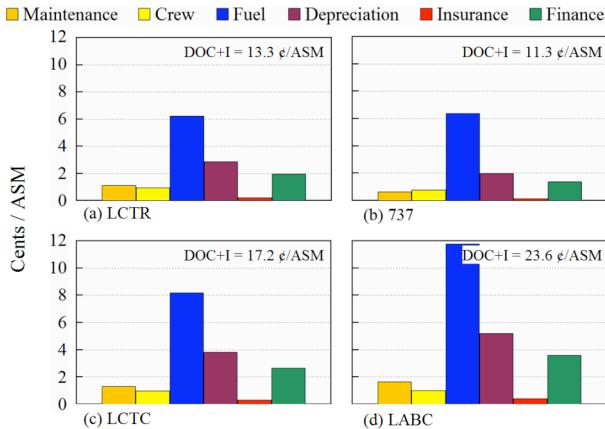
Figure 10. Cost elements compared for heavy-lift rotorcraft and B737 (1,200 nm, 120 passengers, including technology factors for rotorcraft costs).
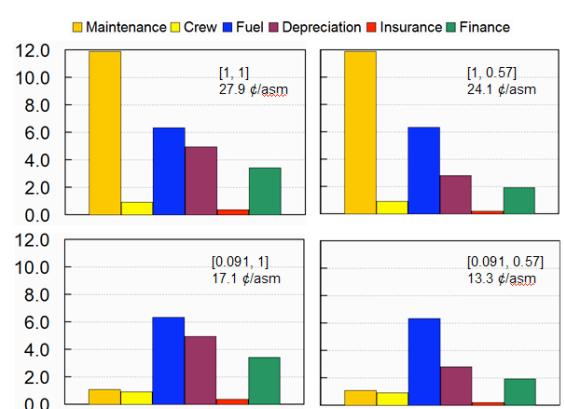
Figure 12. Cost elements compared for LCTR with and without cost technology factors lift rotorcraft (1200 nm, 120 passengers); in legend [x,y], x is maintenance factor and y is price factor.

19
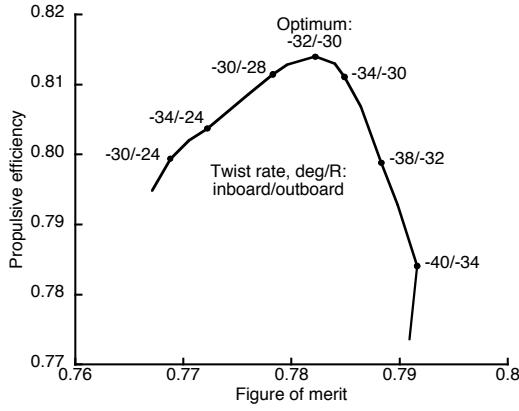
Figure 13. LCTR twist optimization.
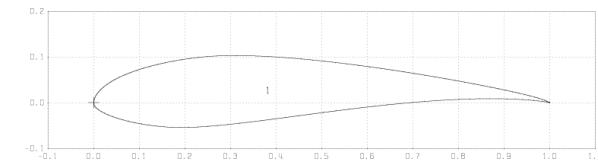
a) Root section: AFDD CTR1544, $c_m = -0.160$, t/c = 15.3%
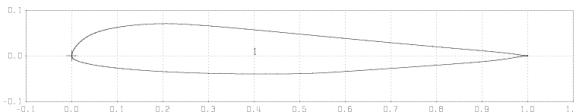
b) Mid-span section: AFDD CTR4475, $c_m = 0.027$, t/c = 11.3%
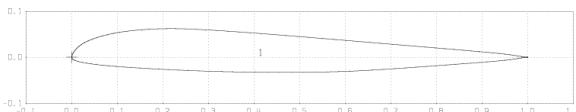
c) Tip section: AFDD CTR7500, $c_m = 0.014$, t/c = 9.0%

Figure 14. LCTR airfoil sections.
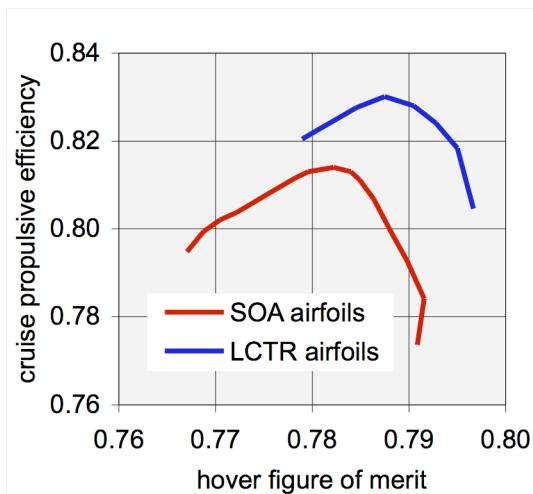
Figure 15. Influence of airfoils on LCTR hover and cruise performance.
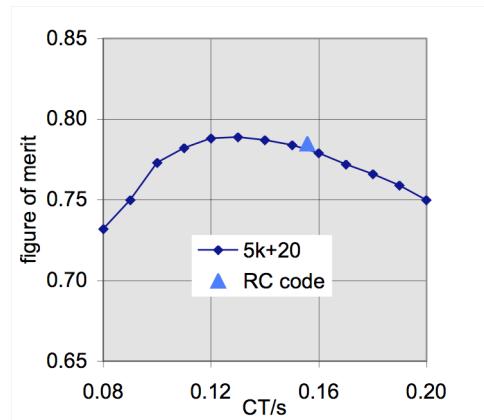
Figure 16. LCTR rotor hover performance.
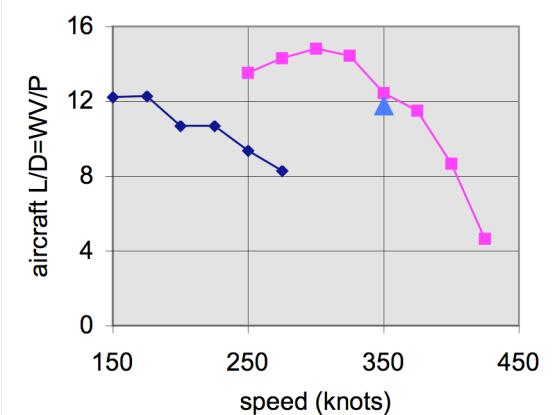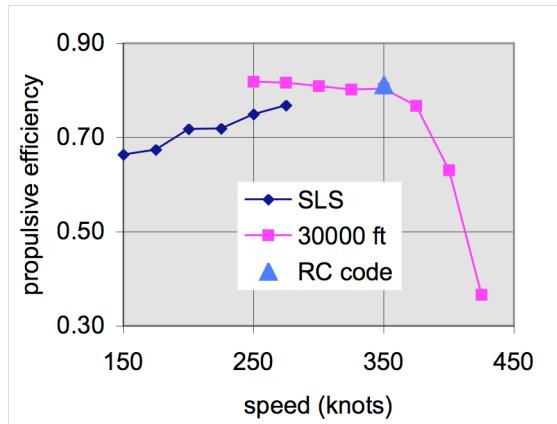
Figure 17. LCTR rotor and aircraft cruise performance.
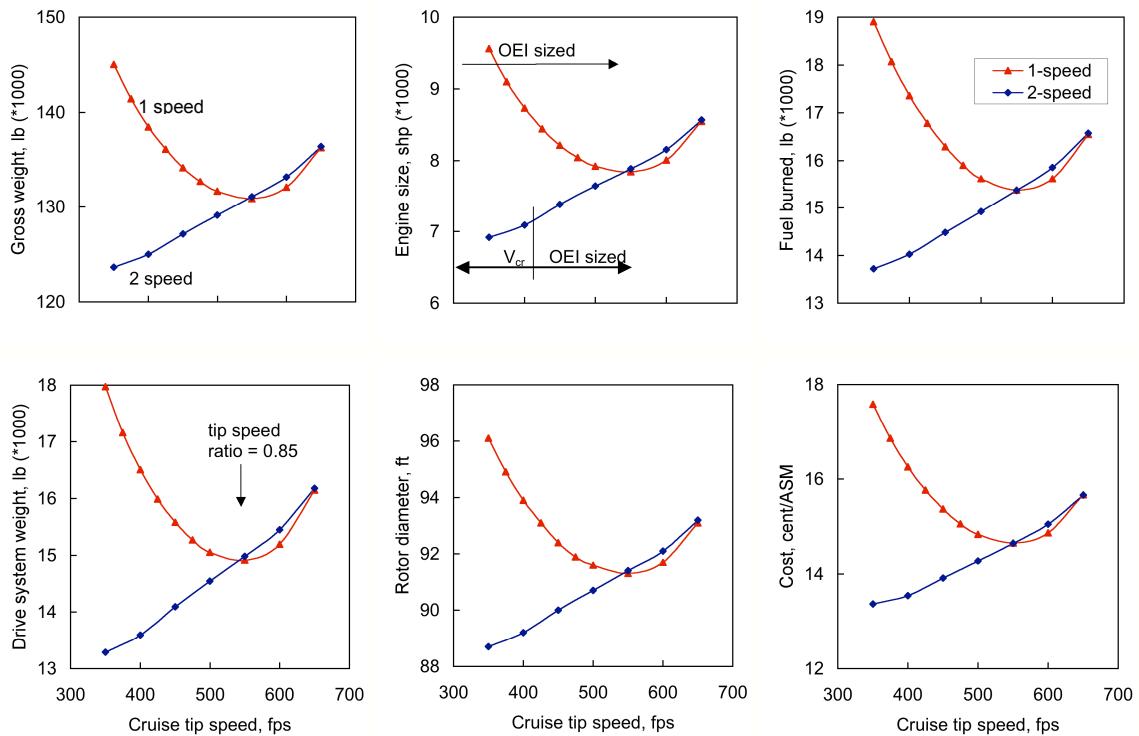
Figure 18. Influence of cruise tip speed on the LCTR design (hover tip speed 650 ft/sec, disk loading 10 lb/ft^2, 4 engines, 4 blades), for 1-speed transmission and for 2-speed transmission.
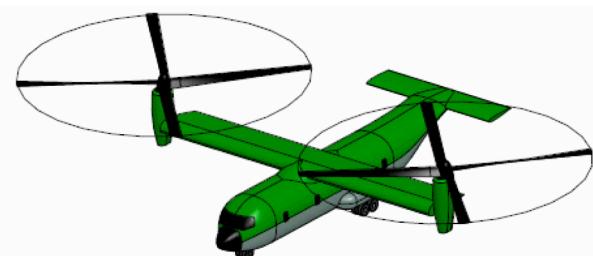
Figure 19. Baseline tiltrotor configuration (courtesy Gerardo Nunez of U.S. Army, AFDD)

Figure 20. Baseline quad tiltrotor configuration (courtesy Gerardo Nunez of U.S. Army, AFDD).
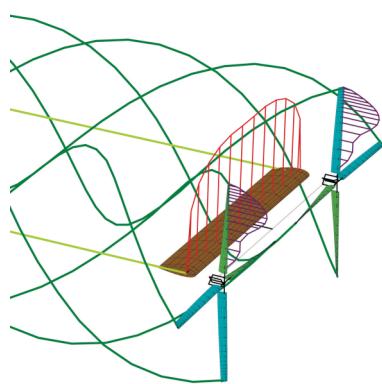
Figure 21. Wake geometry of conventional tiltrotor.
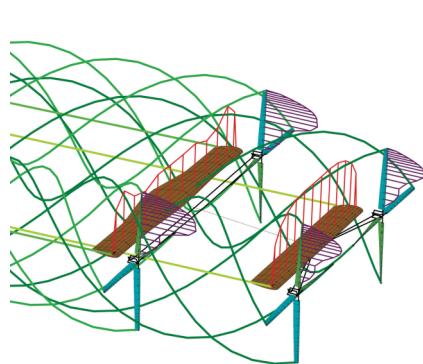
Figure 22. Wake geometry of quad tiltrotor.
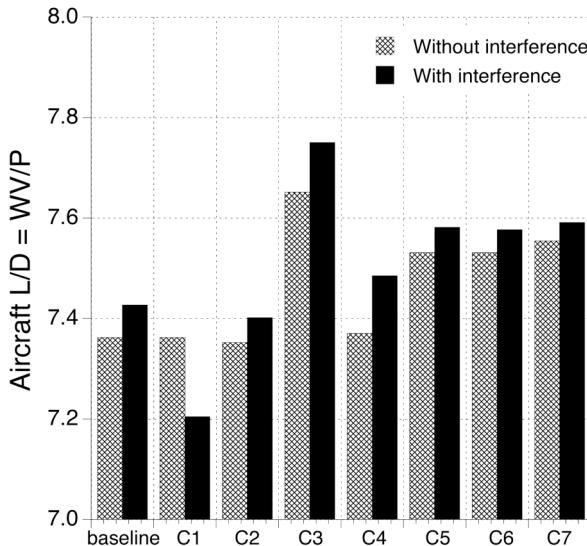
Figure 23. Aircraft lift-to-drag ratio of conventional tiltrotor (with flapping trim).
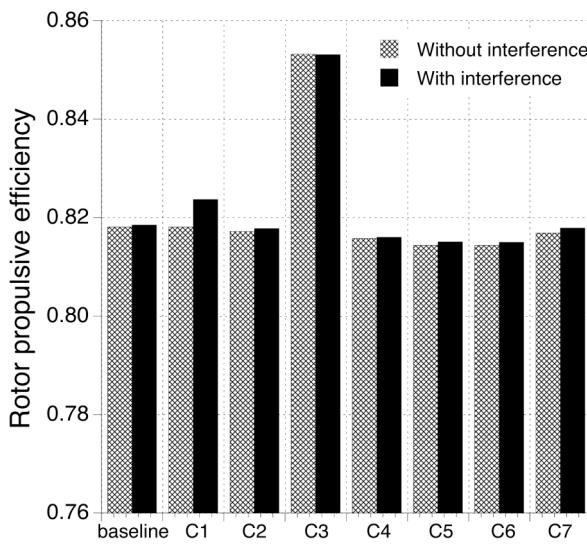
Figure 24. Rotor propulsive efficiency of conventional tiltrotor (with flapping trim).
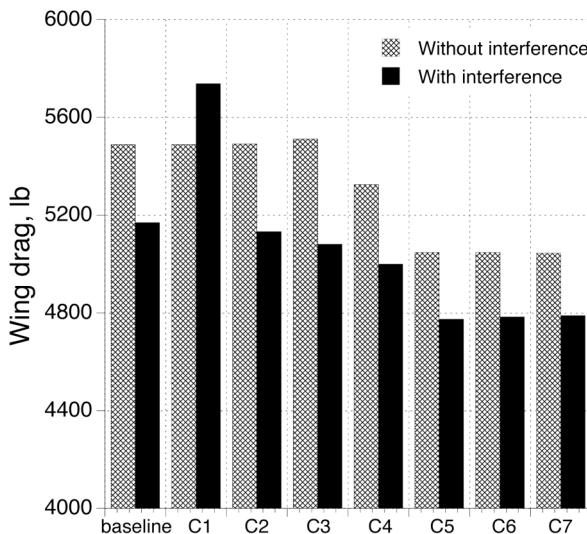
Figure 25. Wing drag of conventional tiltrotor (with flapping trim).
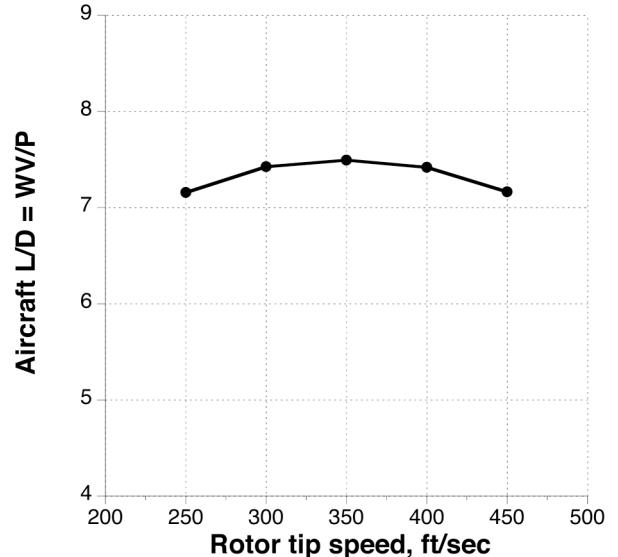
Figure 26. Influence of rotor cruise tip speed on aircraft performance.
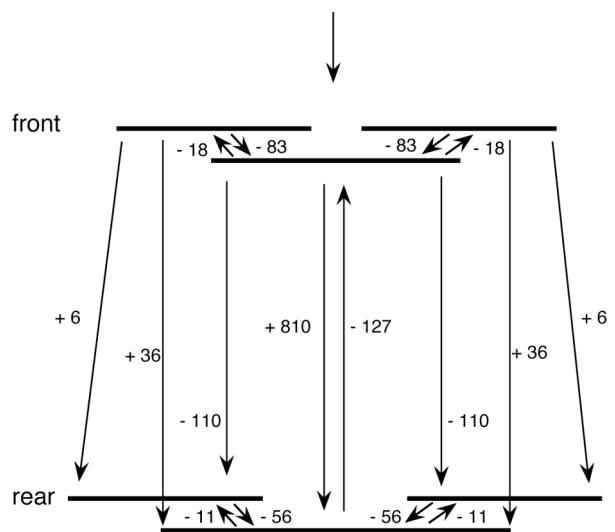
Figure 27. Interference effects on required power of quad tiltrotor (arrowhead indicates component receiving interference; numbers positive for power increase, unfavorable interference; units are HP).
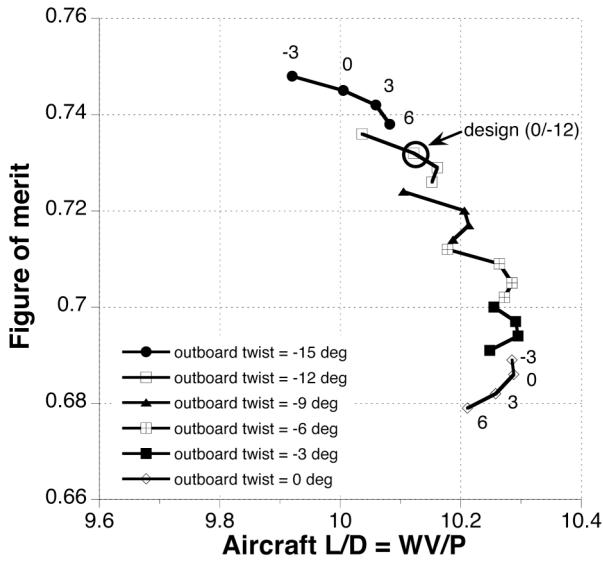
Figure 28. Effect of blade twist on LCTC performance (inboard twist = –3, 0, 3, 6 deg).
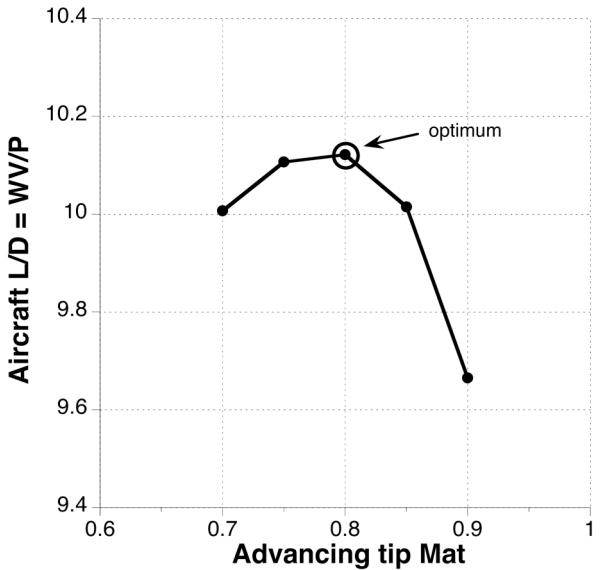
Figure 31. Effect of tip speed on LCTC performance.
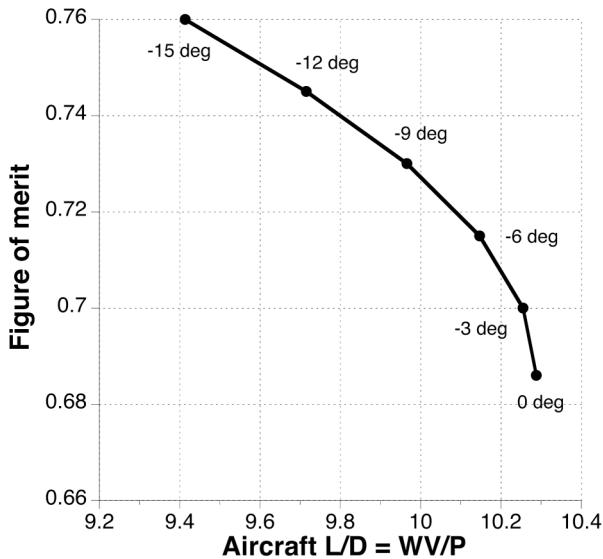
Figure 29. Performance of LCTC with linear twist.
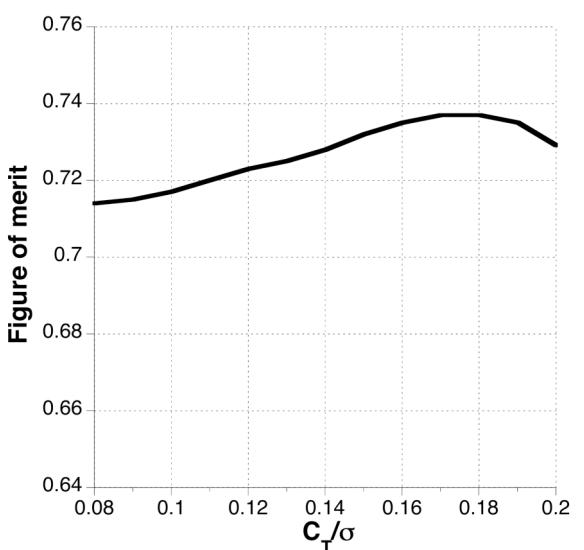
Figure 32. LCTC hover figure of merit.
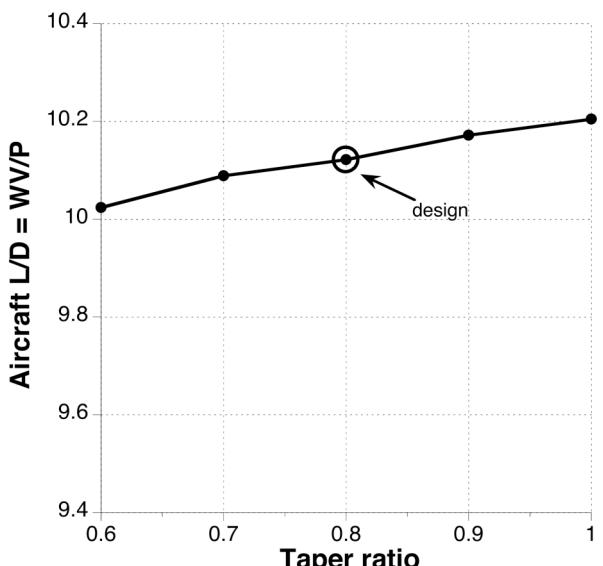
Figure 30. Effect of blade taper on LCTC performance.
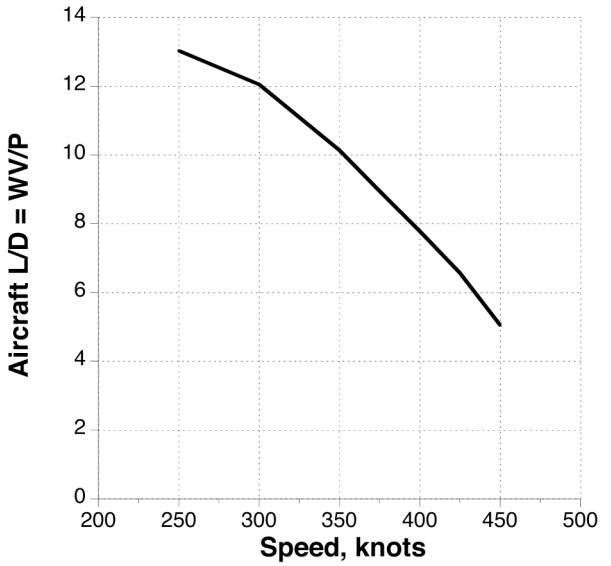
Figure 33. LCTC aircraft cruise performance
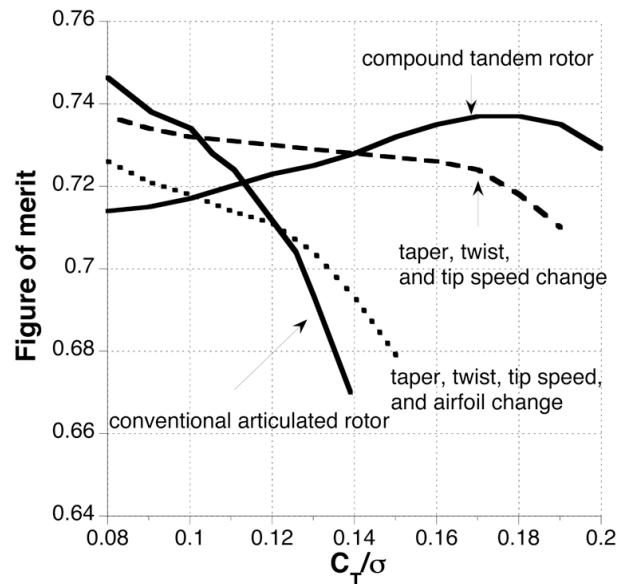
Figure 34. LCTC hover performance buildup. Baseline is compound tandem rotor (using state-of-the-art airfoils). Dashed line uses taper, twist, and tip speed of a conventional articulated rotor. Dotted line also uses airfoils of a conventional articulated rotor.
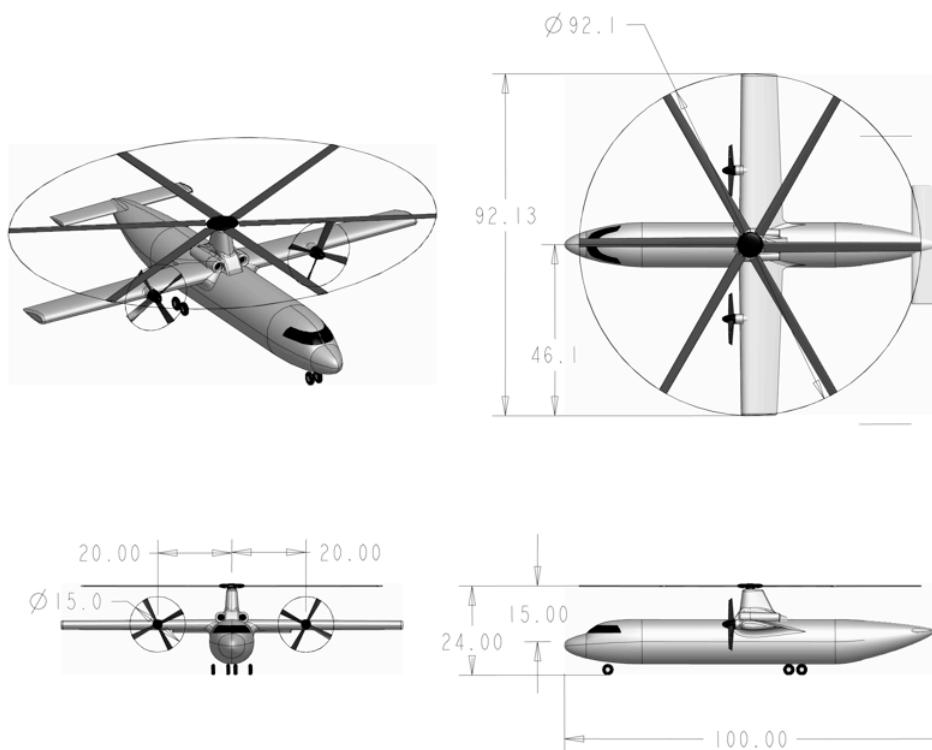
Figures 35. Compound helicopter (courtesy Gerardo Nunez, U.S. Army, AFDD).
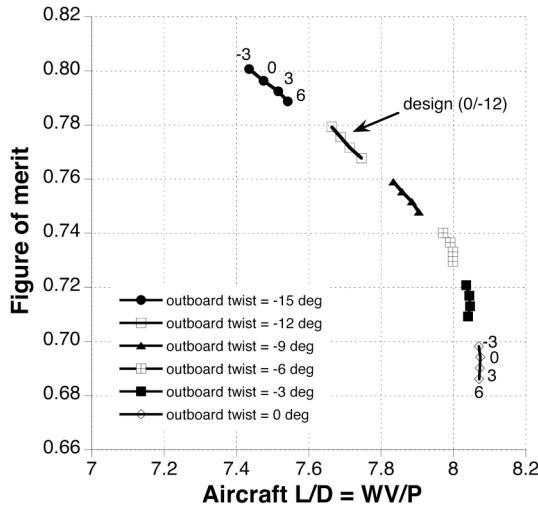
Figure 36. Effect of blade twist on compound helicopter performance (inboard twist = –3, 0, 3, 6 deg).
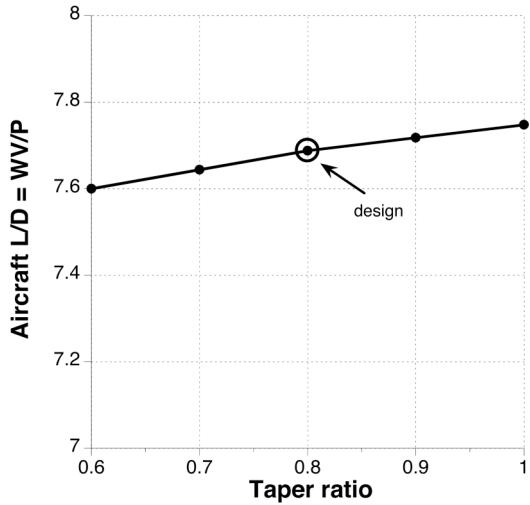
Figure 37. Effect of blade taper on compound helicopter performance.

Figure 38. Effect of cruise tip speed on compound helicopter performance.

Figure 39. Compound helicopter hover figure of merit.
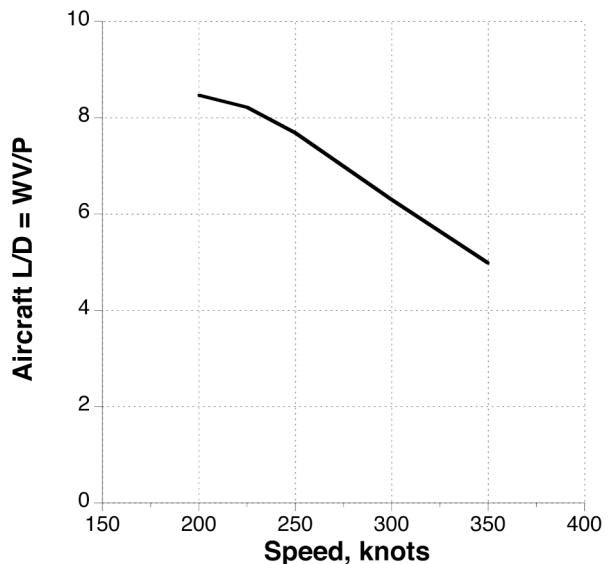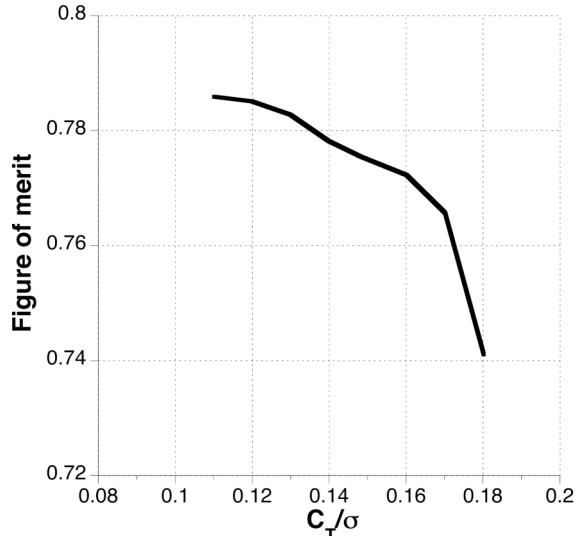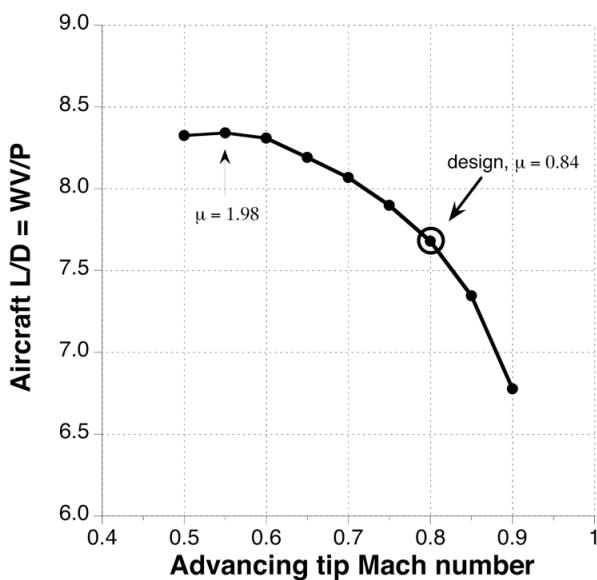
Figure 40. Compound helicopter cruise lift-to-drag ratio.
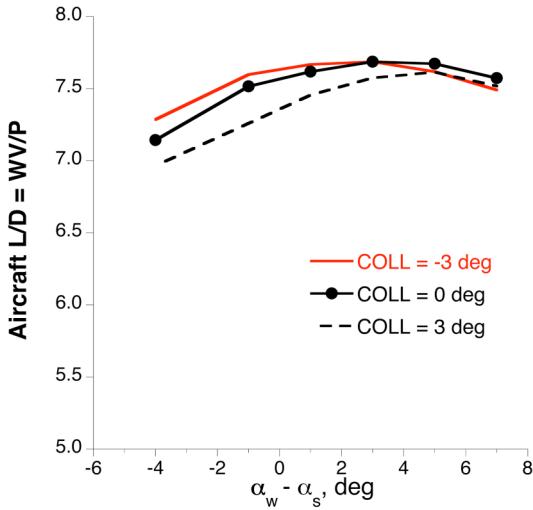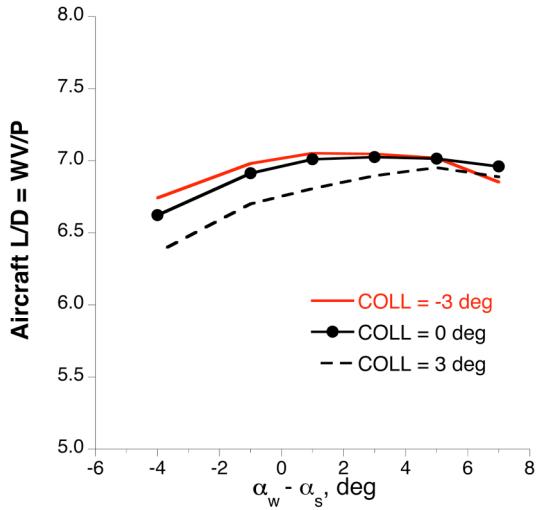
(a) Wing loading W/S = 100   (b) Wing loading W/S = 120

Figure 41. Effect of wing loading on aircraft lift-to-drag ratio (W/A = 15, $C_W/\sigma = 0.14$).
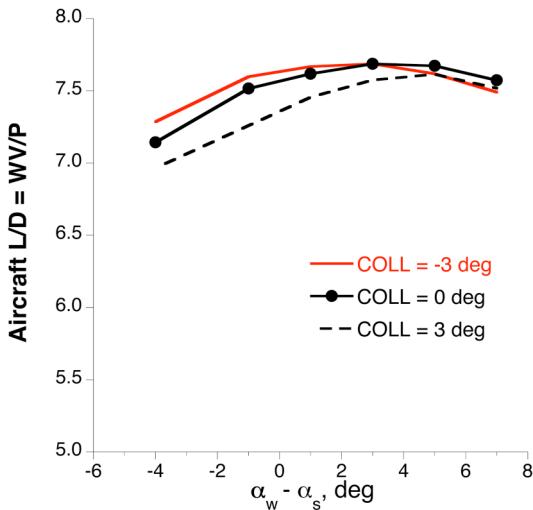
(a) Blade loading $C_W/\sigma = 0.14$ (b) Blade loading $C_W/\sigma = 0.09$
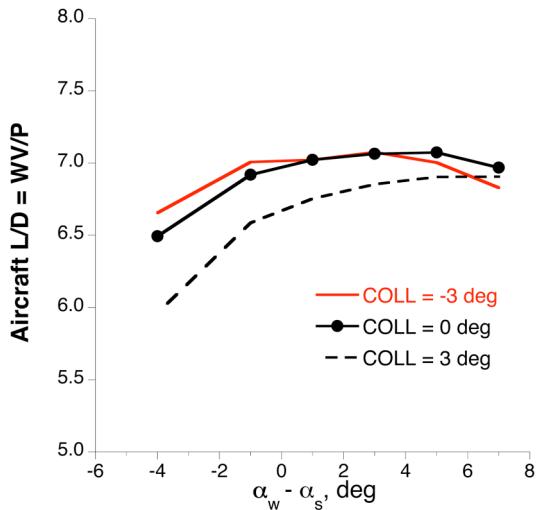
Figure 42. Effect of blade loading on aircraft lift-to-drag ratio (W/A = 15, W/S = 100).
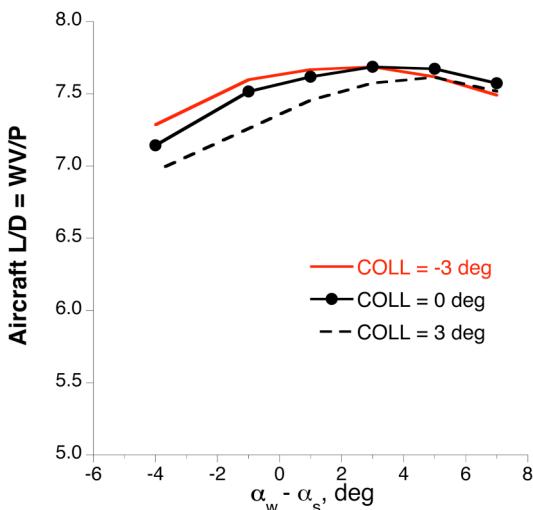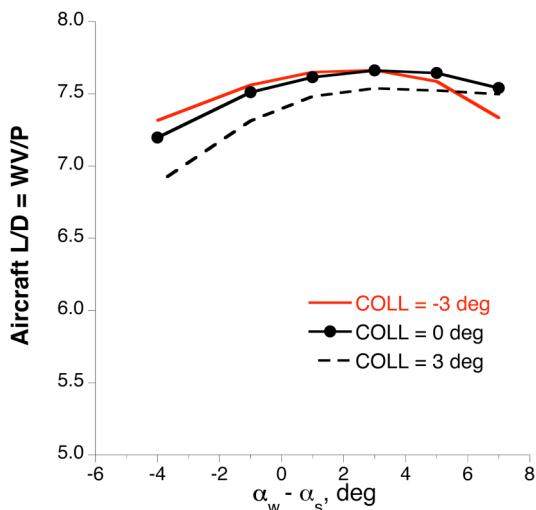
(a) Disk loading W/A = 15   (b) Disk loading W/A = 12

Figure 43. Effect of disk loading on aircraft lift-to-drag ratio ($C_W/\sigma = 0.14$, W/S = 100).
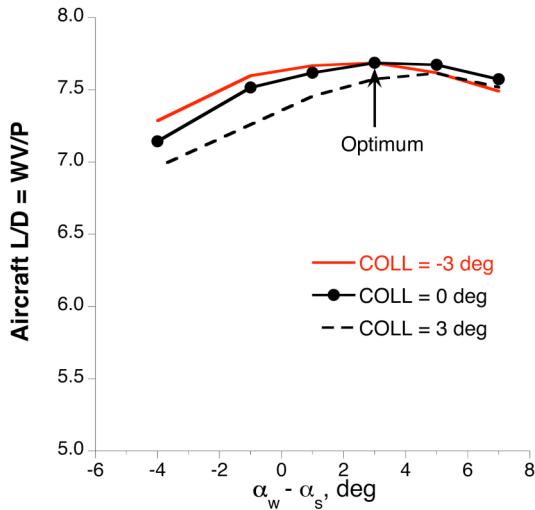
(a) Aircraft lift-to-drag ratio   (b) Rotor shaft power
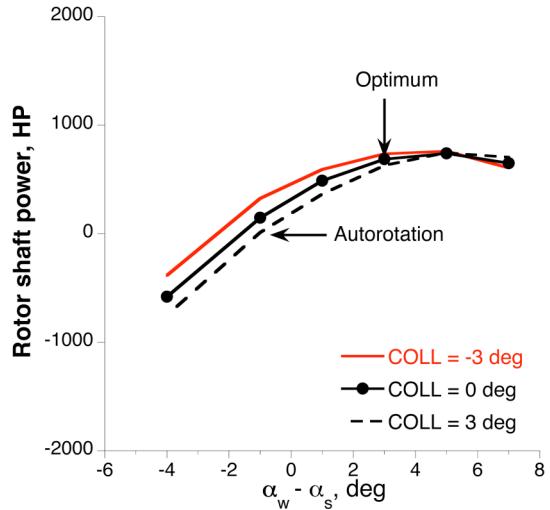
Figure 44. Aircraft lift-to-drag ratio and rotor shaft power (W/A = 15, C_W/σ = 0.14, W/S = 100).
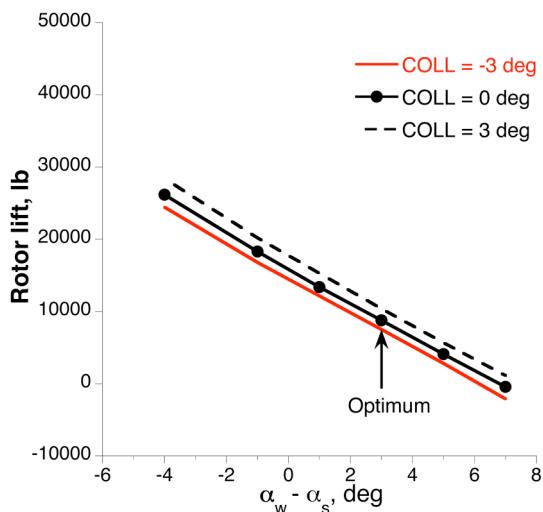
(a) Rotor lift   (b) Wing lift
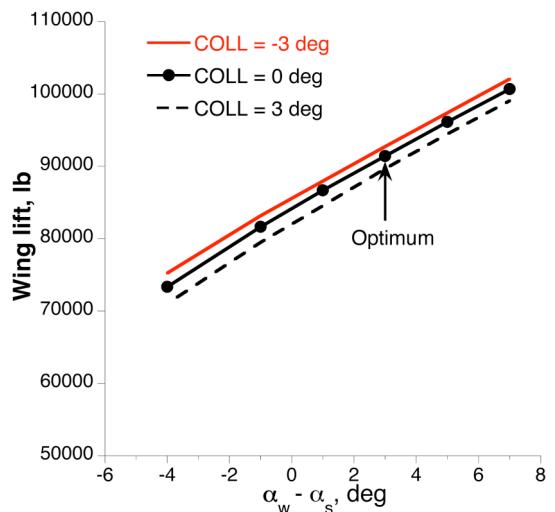
Figure 45. Optimum lift sharing (W/A = 15, C_W/σ = 0.14, W/S = 100).
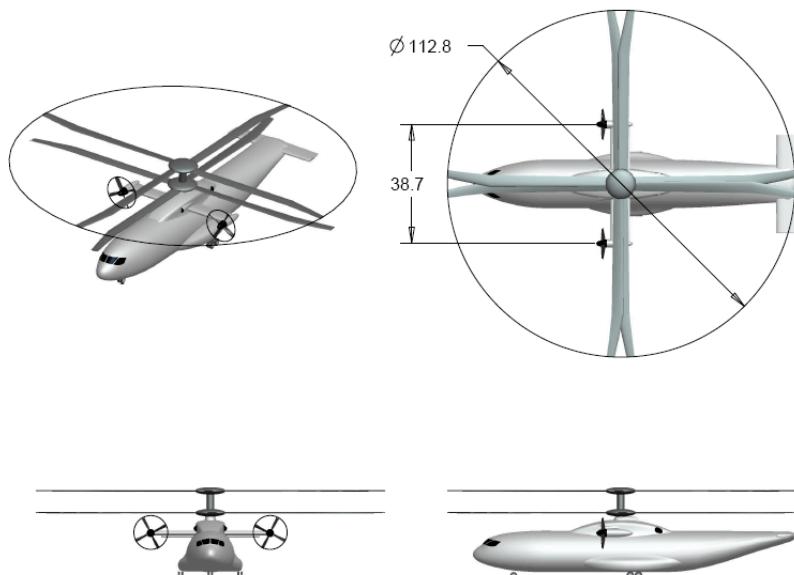
Figure 46. Lift-offset coaxial helicopter (courtesy Gerardo Nunez, U.S. Army, AFDD).
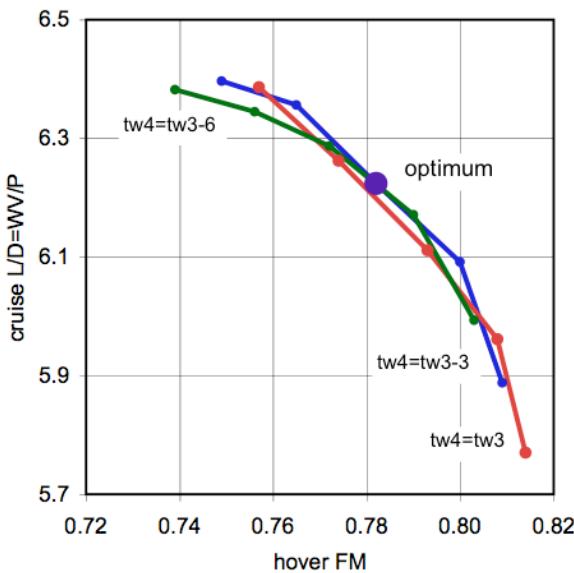
Figure 47. Effect of twist on lift-offset coaxial helicopter performance (twist = linear rate, root to tip). Inboard twist fixed at –3/–6 deg; tw3 extends from 0.5R to 0.75R, tw4 from 0.75R to 1.0R. For each curve, tw4 varies from –12 to –24 deg.


Figure 49. Lift-offset coaxial helicopter rotor effective lift-to-drag ratio, $L/D_e = TV/(P_i+P_o)$ (offset = 0.15, 0.20, 0.25 [design], 0.30).
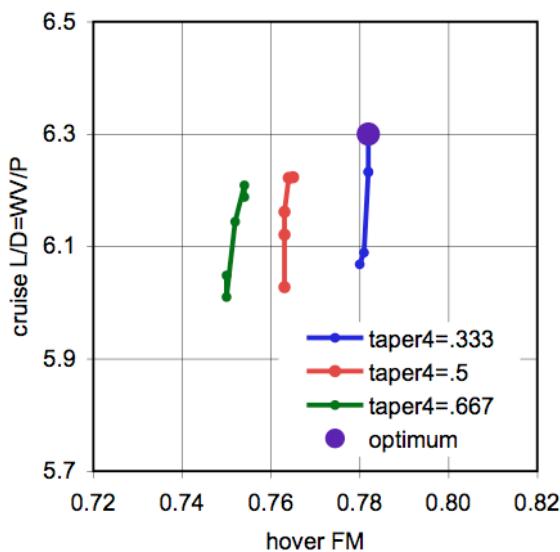
Figure 48. Effect of taper on lift-offset coaxial helicopter performance (taper = tip/root chord ratio). Inboard taper fixed at 1.333; taper3 extends from 0.5R to 0.75R, taper4 from 0.75R to 1.0R. For each taper4 value, taper3 varies from 0.667 to 1.5.
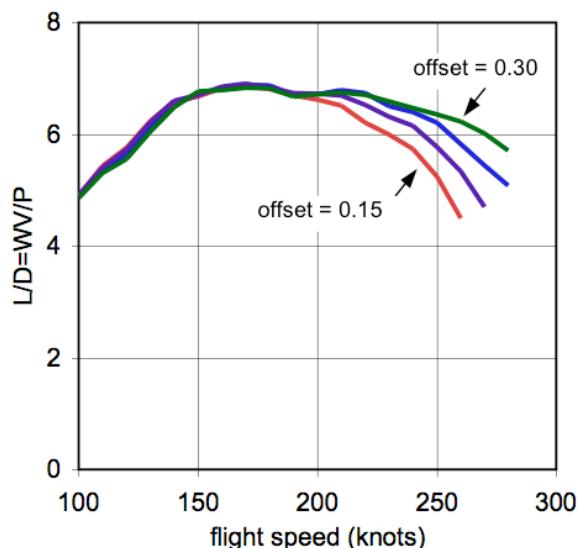

Figure 50. Lift-offset coaxial helicopter aircraft lift-to-drag ratio, $L/D = WV/P$ (offset = 0.15, 0.20, 0.25 [design], 0.30).